ABSORPTION PROPERTIES OF SF_6 NEAR 10.6 μm

ABSORPTION PROPERTIES OF SF_6 NEAR 10.6 μm

by

THOMAS ARVID ZNOTINS, B.Sc.

A Thesis
Submitted to the School of Graduate Studies
in Partial Fulfilment of the Requirements
for the Degree
Master of Science

McMaster University
April 1978

MASTER OF SCIENCE (1978)
(Physics)

McMASTER UNIVERSITY
Hamilton, Ontario

TITLE: Absorption Properties of SF_6 near 10.6 μm

AUTHOR: Thomas Arvid Znotins, B.Sc. (University of Windsor)

SUPERVISORS: Professor B.K. Garside, Professor E.A. Ballik

NUMBER OF PAGES: x, 82

ABSTRACT

The work described in this thesis concerns the investigation of the absorption properties of SF_6 in the 10.4 μm band of CO_2 lasers. Although SF_6 has been used frequently as a saturable absorber in CO_2 laser systems, the complex dynamical behaviour of its absorption was not understood prior to our work. A model is developed which allows for the multilevel nature of the absorption processes. This model treats all the SF_6 vibrational and rotational levels as belonging to a bath of levels characterized by a single vibrational temperature and a single rotational temperature. Energy absorbed from a laser pulse is rapidly distributed throughout this bath, establishing a new vibrational population distribution characteristic of the higher vibrational temperature.

The vibrational equilibrium is readily maintained at high SF_6 pressures. It is demonstrated that in this case the model successfully predicts the transmission and pulse shaping of high power CO_2 laser pulses. In particular, the rapid decrease in absorption at high incident intensities is shown to be due to vibrational heating and not to any intensity saturation process. Dissociation which occurs as a result of sufficient vibrational heating is discussed. The effect of dissociation on single pulse transmission is determined through simple modifications of the model.

The model is also shown to have application to low SF_6 pressures. Previous investigations concerning vibrational relaxation rates in SF_6

would indicate that vibrational equilibrium cannot be maintained in such a situation. More recent results show that in fact sufficiently rapid vibrational energy exchange can occur. The final portion of this thesis discusses the dependence of these rates on the vibrational energy of the molecules. An approximate, but conceptually simple, method of incorporating these effects into the model is described. In conclusion, it is shown that the model is capable of determining the SF_6 absorption behaviour for a wide range of SF_6 pressures and CO_2 laser wavelengths when both intensity saturation and vibrational heating effects are included.

ACKNOWLEDGEMENTS

I wish to express my appreciation to my supervisors, Dr. B.K. Garside and Dr. E.A. Ballik for the guidance, support and encouragement that they have given me throughout the course of this work. I would also like to thank my colleague, Dr. R.S. Taylor, for his important contribution to some of the initial experiments reported in this thesis.

I am indebted to McMaster University for its support in the form of a Teaching Assistantship and to the National Research Council of Canada for a Post-Graduate Scholarship.

I also thank my parents, for things too numerous to mention.

TABLE OF CONTENTS

Page

LIST OF FIGURES

LIST OF TABLES

CHAPTER 1

INTRODUCTION

1.1 SF_6 as a Saturable Absorber

A saturable absorber is a material whose absorption is reduced when the incident light intensity is increased beyond a certain level. The simplest description of this can be given in terms of a transition occurring between two energy levels. Intensity saturation occurs when the absorption rate approaches the rate at which the absorber population can return to equilibrium. Saturable absorbers have been used extensively to produce trains of short duration laser pulses by the technique of passive mode-locking [1]. Mode-locking of a cw CO_2 laser using SF_6 as a saturable absorber was first reported in 1968 by Wood and Schwarz [2]. In 1970, Beaulieu [3] reported laser action from a transversely-excited, atmospheric pressure (TEA) CO_2 laser. Very high pulsed power outputs can be obtained because of the high pressures and large volumes employed. Fortin et al. [4] produced ~1.5 ns duration pulses through SF_6 mode-locking of TEA CO_2 lasers.

Saturable absorbers are also frequently used as optical isolators in high power laser amplifier systems. Parasitic oscillations arising from noise fluctuations can cause substantial depletion of the gain prior to arrival of the actual signal pulse. A saturable absorber inserted into the beam path can prevent amplification of these low intensity fluctuations and yet permit high transmission of high intensity pulses. Large, high-power amplification systems are generally associated with laser induced thermonuclear fusion research. An example is the 100 KJ CO_2 laser fusion system currently under construction at the Los Alamos Scientific Laboratories. Considerable research is presently underway to determine the suitability of low pressure SF_6-based gas mixtures to serve as isolators in such systems [5,6].

Another saturable absorber used with CO_2 lasers is p-type Ge [5,7]. The chief advantage of Ge over SF_6 as a CO_2 mode-locker is in the production of extremely short laser pulses by Ge due to the very fast relaxation rates present [8]. In addition, Ge can be used in multi-line and multi-band application; the resonant nature of SF_6 absorption restricts it to essentially single-line operation. This difficulty can be overcome through the use of gas mixtures.

A major advantage of gaseous saturable absorbers is their high damage threshold, limitations actually being determined by the absorption cell windows. For NaCl the threshold is ≥5 J/cm^2 [9]. Recently, Delichatsios et al. [10] reported a high pressure gas isolator technique in which the gas mixture is flowed across the beam path. This eliminates the need for cell windows altogether. Many other polyatomic molecules, such as BCl_3 [11], N_2F_4 [11], CCl_3F [12], and CH_3CHF_2 [13], have been employed as saturable absorbers for CO_2 lasers. However, SF_6 remains the one most commonly used, not only because of its very large absorption, but also because it is non-caustic, non-toxic, non-flammable, essentially non-reactive, relatively inexpensive, and readily available. Therefore, it is important to understand the absorption properties of SF_6 over a wide range of operating conditions. Furthermore, the behaviour of SF_6 is indicative of the response of the other large polyatomic molecules that interact with CO_2 laser radiation.

Laser induced, multiphoton dissociation of polyatomic molecules (such as SF_6) is of considerable present interest [14,15], especially since it has been demonstrated that the process is isotopically selective [16]. However the means by which this dissociation occurs remains unclear. Studies of the saturation behaviour of SF_6 provide information concerning the vibrational relaxation rates which are essential to any explanation of the multiphoton process.

1.2 Outline of the Contents of the Thesis

The emphasis of this work is on the development of a model which is able to describe the absorption properties of SF_6 over a wide range of CO_2 laser wavelengths and SF_6 gas pressures. The model, referred to throughout this work as the vibrational bath model, incorporates the multilevel nature of the absorption processes present in polyatomic molecules such as SF_6.

Chapter 2 describes the development of the basic model and its ability to predict SF_6 absorption as a function of vibrational temperature. The model is found to be applicable even at low pressures, which provides evidence for the existence of very rapid vibrational energy exchange rates in SF_6. In Chapter 3 it is shown that the vibrational bath model can accurately predict the transmission and pulse shaping of single pulses propagating through high pressure SF_6. In addition, it is demonstrated that the disappearance of absorption at large input intensities occurs because of vibrational heating and is not due to any intensity saturation process.

Chapter 4 considers the dissociation which occurs due to this vibrational heating. The model is modified to predict the magnitude of the dissociation observed and to account for the effect of this on single pulse transmission. In Chapter 5 experimental evidence is reported which demonstrates the dependence of the vibrational relaxation rates on the degree of vibrational excitation. The bath model is modified to account for the essential features of the saturation behaviour observed at low SF_6 pressures.

CHAPTER 2

THE VIBRATIONAL BATH MODEL

2.1 Introduction

The interaction between an atomic or molecular system and electromagnetic radiation can often be described in terms of a simple 2 or 4-level model. This cannot be done with large polyatomic molecules as can be seen from the inability of these models to describe adequately the dymanics of SF_6 absorption [17,18]. Early experiments showed that substantial absorption can occur from levels other than those at or near the ground state. Recently, work in the area of multiphoton dissociation of polyatomic molecules such as SF_6 has demonstrated that absorption can occur even from regions of very high vibrational excitation, which can extend beyond the dissociation limit.

There is much current interest in understanding the processes in which vibrational energy can be redistributed within a molecule as the energy is being absorbed from a laser pulse. At low pressures there is evidence that the absorbed energy is transferred to a large number of vibrational levels via very rapid intramolecular, radiationless, collisionless, vibration-to-vibration (V-V) processes [19]. At progressively higher gas pressures collision-dependent intermolecular processes dominate in V-V energy exchanges [20]. These energy exchange processes are sufficiently fast, in comparison with the duration of a Q-switched CO_2 laser pulse, to allow construction of an absorption model for SF_6 in which the many vibrational and rotational levels are considered as belonging to a population distribution characterized by vibrational and rotational temperatures, T_V and T_R, respectively. Energy from an incident laser pulse is absorbed into the complex multilevel system and heats the entire vibrational mode, resulting in a new higher effective bath temperature. The absorption appropriate to this new temperature can be calculated for all the CO_2 P-lines once the SF_6 gas cell thickness, the gas pressure, the transmitted pulse intensity, and the input pulse duration are known. Provided that equilibrium conditions for the vibrational levels are met, the model can predict the time dependence of the absorption on all CO_2 P-lines (except the input pulse) during the input pulse duration. It is shown in Chapter 3 that, at high SF_6 pressures, the model can correctly predict the entire transmission and pulse shaping behaviour of the input pulse itself from low transmittances to very high transmittances. The model is particularly applicable at high pressures since at these pressures (typically >200 Torr) the increase in pulse transmission due to vibrational heating dominates over the contribution by true intensity saturation processes. The situation at low pressures is somewhat more complicated and is discussed in Chapter 5.

2.2 Development of the Vibrational Bath Model

SF_6 is an octahedral molecule having 15 vibrational degrees of freedom distributed among 6 fundamental modes of vibration. Figure 2-1 shows a portion of the vibrational energy level diagram for SF_6. Absorption from the ground state to the ν_3 fundamental (948 cm^{-1}) is indicated by the solid arrow. The subsequent relaxation processes, V-V (vibration-

Fig. 2-1

Energy level diagram for SF_6.

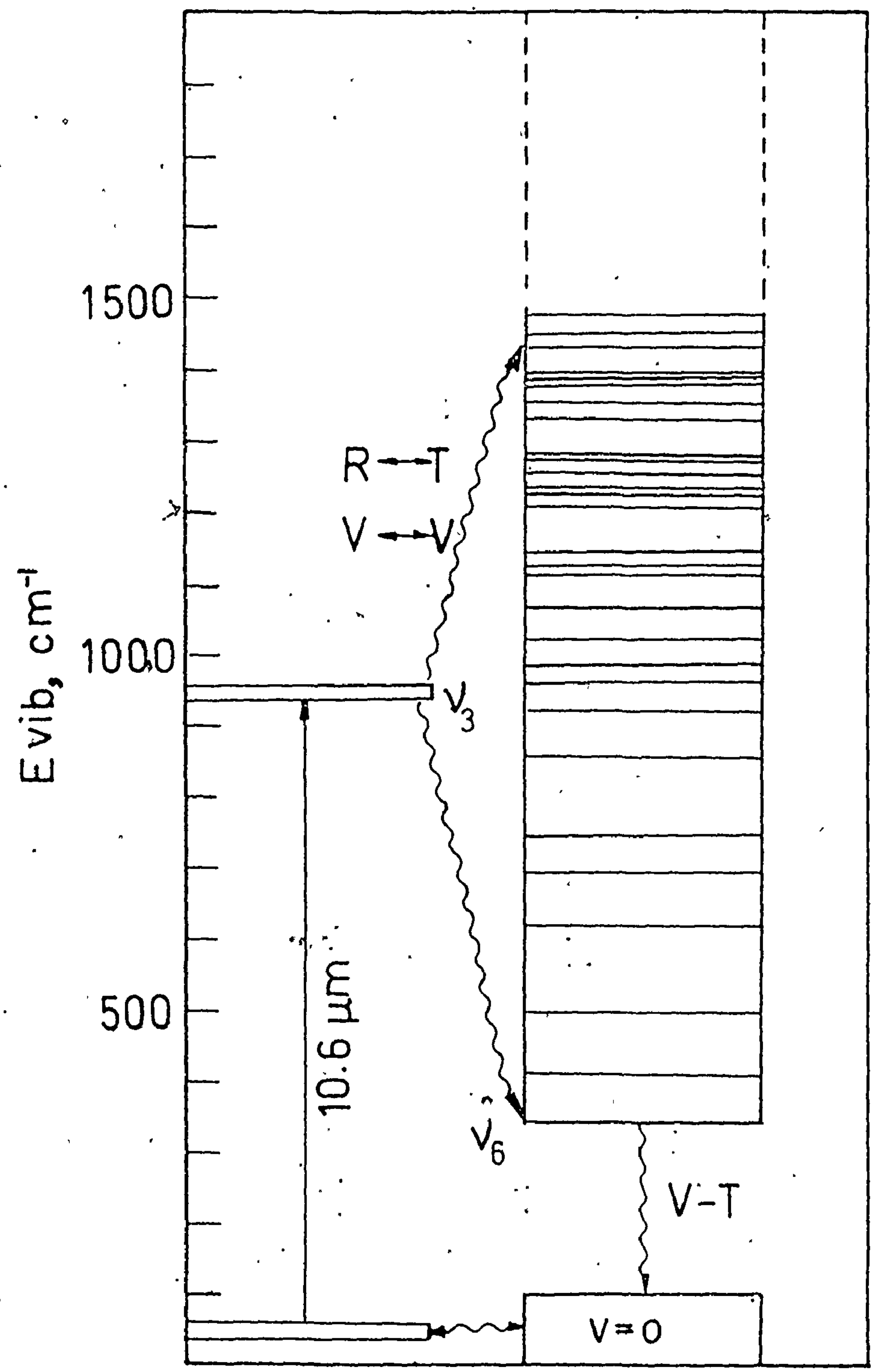
1500
1000
500
E vib, cm-1
R ⟷ T
V ⟷ V
ν3
ν6
10.6 μm
V-T
V=0

to-vibration), V-T (vibration-to-translation) and R-T (rotation-to-translation) are indicated by wavy lines. Note that the density of states begins to increase rapidly beyond 1000 cm^{-1}. The intensity of an absorption from any one of these vibrational states ℓ to an upper state u can be expressed as [21]

$$k_{\ell u}(\nu) = \frac{8\pi^3 \nu_{\ell u}}{3hc} |<\ell|\mu|u>|^2 [1 - \exp(\frac{-h\nu_{\ell u}}{KT_V})] N_\ell f(J,T_R) \quad , \qquad (2\text{-}1)$$

where N_ℓ refers to the population of the lower state. Here the quantity $f(J,T_R)$ involves the rotational dependence and has the form [22]

$$f(J,T_R) = A_{J,\nu} g_J Q_J^{-1} \exp(\frac{-BJ(J+1)hc}{KT_R}) \quad , \qquad (2\text{-}2)$$

where Q_J is the rotational partition function, g_J the degeneracy of the rotational level, and $A_{J,\nu}$ the transition amplitude, which for octahedral molecules has the value [23]

$$A_{J,\nu} = \frac{2J-1}{2J+1} \qquad \text{P-branch}$$

$$A_{J,\nu} = 1 \qquad \text{Q-branch}$$

$$A_{J,\nu} = \frac{2J+3}{2J+1} \qquad \text{R-branch}$$

The contribution of all the rotational lines that can absorb within a linewidth $\Delta\nu$ is included by means of a scale factor $\Delta\nu/|\Delta\nu_J|$, where $\Delta\nu_J$ is the spacing between adjacent rotational lines in the neighbourhood of a given J. The product of this scale factor and $f(J,T_R)$ can be considered as an effective rotational cross-section. For the case of SF_6 it is found to be a slowly varying function of rotational temperature as is discussed in the next section.

Be regarding the ν_3 mode as an independent harmonic oscillator, it can be shown that

$$|\langle \ell|\mu|u\rangle|^2 = \frac{h}{8\pi^2 c\nu_{\ell u}} \left(1 + \frac{v_3}{3}\right)\left(\frac{d\mu}{dQ_3}\right)^2 , \qquad (2\text{-}3)$$

where v_3 is the number of ν_3 quanta present in the lower level. The factor 1/3 accounts for the 3-fold degeneracy of the ν_3 mode.

Using the value of $d\mu/dQ_3$ given in Ref. [24] and setting $\nu_{\ell u}$ equal to the ν_3 fundamental, results in

$$|\langle \ell|\mu|u\rangle|^2 = (1.50 \pm 0.15) \times 10^{-37} \ (\text{esu-cm})^2 .$$

Substituting in the standard Boltzmann expression for N_ℓ and summing the contributions from the vibrational (E_V) and rotational (J) levels involved, as given by Eq. (2-1), yields the total absorption coefficient

$$\alpha(\nu)\Delta\nu = (1.91 \pm 0.20) \sum_{E_V} \left[1 - \exp\left(-\frac{h\nu}{KT_V}\right)\right]\left(1 + \frac{v_3}{3}\right) g(E_V) Q_V^{-1} \qquad (2\text{-}4)$$

$$\times \exp\left(-\frac{E_V}{KT_V}\right) \sum_J Q_J^{-1} A_{J,\nu} (2J + 1)^2 \left|\frac{\Delta\nu}{\Delta\nu_J}\right| \exp\left[-\frac{BJ(J+1)hc}{KT_R}\right] ,$$

in units of cm^{-1} $Torr^{-1}$. The summation is to be evaluated for all J values at each value of E_v.

The values of J to be summed over at any vibrational level can be obtained in the following manner. The frequency of a ν_3 transition from a particular vibrational level represented by a set of quantum numbers $\{v_i\}$, is [22]

$$\nu\{v_i\} = \nu_o + 2X_{33}v_3 + \sum_{i\neq 3} X_{3i}v_i \quad , \tag{2-5}$$

where ν_o is the ground state transition frequency and the X_{3i} the anharmonicity coefficients.

The transition frequencies for the various branches are then obtained from

$$\begin{aligned}
\nu(P) &= \nu\{v_i\} - (B_3 + B_o - 2B\zeta_3)J + (B_3 - B_o)J^2 \quad , \\
\nu(Q) &= \nu\{v_i\} - (B_3 - B_o)J(J + 1), \text{ and} \\
\nu(R) &= \nu\{v_i\} + (B_3 + B_o - 2B\zeta_3)(J + 1) + (B_3 - B_o)(J + 1)^2 \ .
\end{aligned} \tag{2-6}$$

SF_6 has a very small rotational constant B. Therefore, the separation of rotational levels is such that, within the limits of the model, J can be considered as a continuous variable. Hence the summation over J in Eq. (2-4) is over all the positive real solutions of Eq. (2-6) when the frequency for the particular branch is set equal to that of the laser line.

The exact summation over all the levels of the vibrational bath is a formidable task due to the high density of states in SF_6.

To simplify calculations, all vibrational levels above 2000 cm^{-1} are represented by a grid of single levels having a constant separation of 20 cm^{-1}. The "degeneracy" of each level in this grid is the total number of vibrational states within the 20 cm^{-1} interval. The Whitten-Rabinovitch method for evaluating the sums and densities of molecular states [25] has been successful in obtaining both this degeneracy and also the average values of the quantum numbers in those levels. Details of the Whitten-Rabinovitch method are outlined in the Appendix. The vibrational levels are considered discrete up to 2000 cm^{-1} as the number of states in this region is still sufficiently low for practical calculation of the absorption coefficient as given by Eq. (2-4).*

It is apparent from Eqs. (2-5) and (2-6) that, for a given frequency ν, the effect of the anharmonicities becomes so great that it is not possible to maintain a resonance by rotational compensation in the R-branch. There then exists a point in the bath above which the effective cross-section should vanish. Recently, it has been shown that a finite cross-section, indpendent of the CO_2 laser frequency, does exist for regions high up in the vibrational bath [26]. This cross-section has been attributed to the very high density of states occurring in this quasi-continuum region, and is estimated to be $\sim 4.0 \times 10^{-19}$ cm^2 [27] ($\sim$50 times smaller than typical cross-sections for near resonant levels lower in the bath). This value is used in the model for all levels above that point in the vibrational bath for which rotational compensation for anharmonicity can no longer maintain a

*Jensen et al. [28] have recently calculated the anharmonic splittings of SF_6. Including such splittings in the bath model might give a small improvement in the accuracy of the model, but at the cost of considerably increased calculational complexity.

resonance.

The model also includes the contribution of the $S^{34}F_6$ isotope to the absorption spectrum. The ν_3 band contour is assumed to be identical to that of $S^{32}F_6$, but is shifted to a lower frequency by 17.4 cm^{-1} [24]. The contribution becomes significant for CO_2 lines beyond P(28).

The summation in Eq. (2-4) can now be evaluated over the entire vibrational bath to obtain the total absorption coefficient at a given frequency. In addition, a partial sum can be evaluated for any particular region to determine the absorption occurring there.

2.3 Calculation of Small Signal Absorption

Values for all the spectroscopic constants required were obtained from Ref. [24]. The anharmonicity coefficients were varied within their experimental uncertainties until the best overall fit to the 300 K absorption spectrum of SF_6 was obtained for the wavelength region containing the P(14) to P(32) CO_2 laser lines. The final values employed in the calculations are (in cm^{-1}) $X_{31} = -2.1$, $X_{32} = -1.4$, $X_{33} = -2.6$, $X_{34} = -1.5$, $X_{35} = -1.5$ and $X_{36} = -1.0$. Similarly, a value of 1.91 for the constant in Eq. (2-4) was found to give the best fit to the experimental data over the range specified above. These adjusted coefficients, and all other spectroscopic constants, were not allowed to vary for all the remaining comparisons. Table 2-1 compares the calculated small signal absorption coefficients, at a temperature of 300 K with the experimental values obtained from Refs. [20] and [29].

Figure 2-2 displays the predicted absorption coefficient for

Table 2-1

SF_6 small signal absorption coefficients in units of cm^{-1} $Torr^{-1}$.

CO_2 laser line (10.6 μm band)	Calculated	Measured Ref. [20]	Measured Ref. [29]
P(12)	0.22	0.24	0.24
P(14)	0.45	0.44	0.42
P(16)	1.06	0.97	0.96
P(18)	0.60	0.65	0.58
P(20)	0.55	0.54	0.52
P(22)	0.37	0.37	0.33
P(24)	0.20	0.20	0.19
P(26)	0.098	0.097	0.108
P(28)	0.040	0.045	0.046

Fig. 2-2

Absorption coefficient as a function of vibrational temperature for selected CO_2 rotational lines.

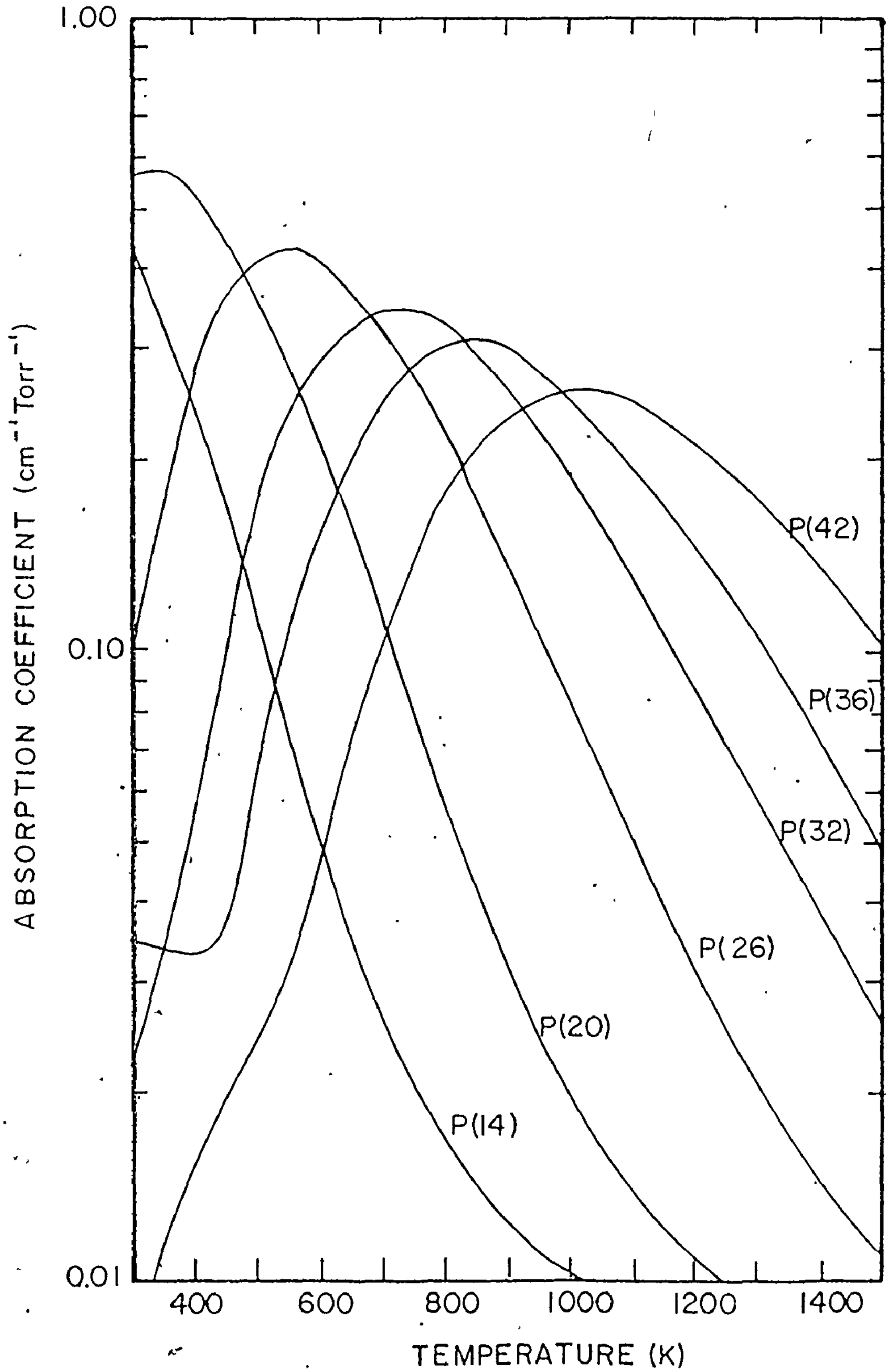
1.00
0.10
0.01
400
600
800
1000
1200
1400
TEMPERATURE (K)
ABSORPTION COEFFICIENT (cm⁻¹Torr⁻¹)
P(42)
P(36)
P(32)
P(26)
P(20)
P(14)

various CO_2 P-lines against vibrational temperature. The decrease in absorption coefficient at the shorter wavelength lines and the initial increase at longer wavelengths is simply due to the shift in the vibrational population distribution to levels farther removed from the ground state, and to regions where anharmonicities favour the longer wavelength CO_2 lines. This is demonstrated in Fig. 2-3 which shows the calculated energy above the ground state for which the effective absorption cross-section (defined in Section 2.2) is a maximum for a given CO_2 P value. This figure indicates the shift in the position for maximum cross-section to higher vibrational levels with progressively longer CO_2 wavelengths. Furthermore, it shows that there are two, and sometimes three maxima, for a given CO_2 P-line which are approximately separated in energy by the energy of a 10.4 μm photon, which correspond to P, Q and R branch rotational transitions. The widths of the P, Q and R cross-section maxima are quite large and can extend for many hundreds of cm^{-1}. These curves demonstrate the possibility of climbing the vibrational energy ladder employing multiple photon absorption processes. This is possible through a compensation for anharmonicities by proceeding through P to Q to R-branch rotational transitions. This mechanism has been discussed in Ref. [30]. It is evident that the P(16) CO_2 line should be able to reach $E_{vib} \sim 2000\ cm^{-1}$ by a 2-photon process, i.e., a Q-branch followed by an R-branch transition. Lines with P number greater than P(18) that have P, Q and R branches allow for the possibility of 3-photon absorption processes.

Also shown in Fig. 2-3 are similar P, Q and R curves for $S^{34}F_6$ molecules. There is an interesting change in the number of multiple

Fig. 2-3

Vibrational energy (above the ground state) for P, Q and R cross-section maxima as a function of CO_2 wavenumber.

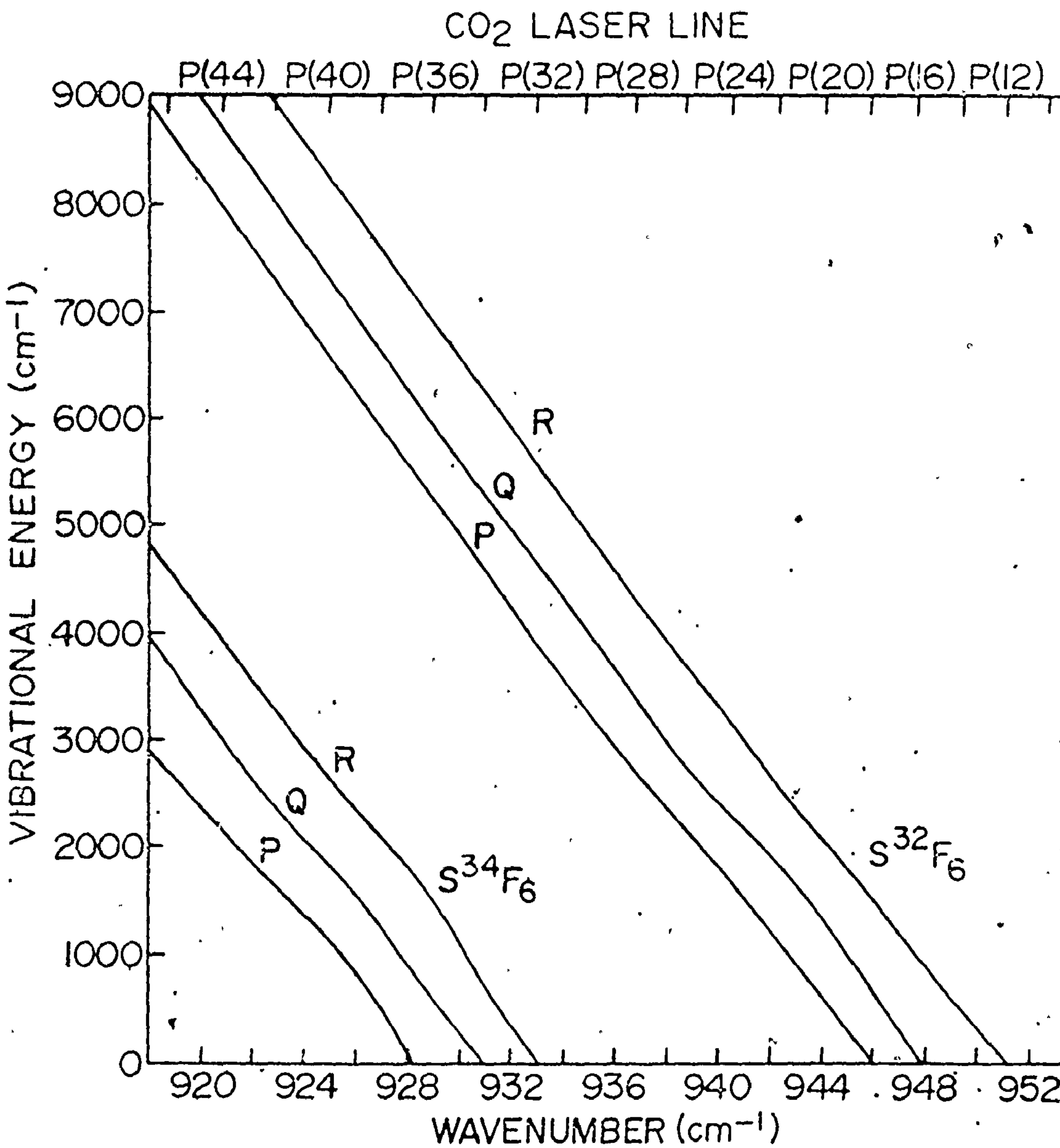
CO2 LASER LINE
P(44) P(40) P(36) P(32) P(28) P(24) P(20) P(16) P(12)
9000
8000
7000
6000
5000
4000
3000
2000
1000
0
VIBRATIONAL ENERGY (cm-1)
R
Q
P
R
Q
P
S34F6
S32F6
920 924 928 932 936 940 944 948 952
WAVENUMBER (cm-1)

absorption steps possible for a P(30) compared to a P(32) CO_2 rotational line. The model-based absorption spectrum for the P(30) line at 300 K indicates that there is only a 10% absorption contribution from $S^{34}F_6$ molecules and that most of the absorption (~70%) occurs from P-branch $S^{32}F_6$ transitions originating at ~2000 cm^{-1} above the ground state. Therefore, for P(30) a possible multiple photon process would consist of a P-branch transition from ~2000 cm^{-1} to ~3000 cm^{-1}, followed by the P to Q to R sequence of transitions suggested by the $S^{32}F_6$ curves. The second P-branch transition is possible due to the large width of the P-branch cross-section maximum. This mechanism for the P(30) multiple photon absorption appears more appropriate than that proposed in Ref. [31].

For the P(32) line, however, 90% of the absorption at 300 K is due to $S^{34}F_6$ molecules in states <1000 cm^{-1}. Presumably, the P(32) absorption process can only consist of an R-branch transition which cannot connect with the region where there is significant P-branch $S^{32}F_6$ cross-section. This is true even when SF_6 pressures are high enough to allow effective collisional interaction between the two isotopic species. However, multiphoton transitions involving stepping from excited $S^{34}F_6$ to $S^{32}F_6$ should be possible if the gas is vibrationally heated so that most of the $S^{34}F_6$ absorption occurs around 3000 cm^{-1}. This argument indicates the importance of considering vibrational heating effects when one speculates on multiphoton absorption processes for different CO_2 lines.

It is important to note that the rotational temperature was maintained at 300 K for all calculations as these calculations are found to be relatively independent of the rotational temperature. This occurs for the following reasons: Although direct vibration-to-rotation (V-R) energy transfer processes are expected to be slow [32], heating of the rotational degrees of freedom may occur via V-T-R processes, but only at sufficiently high SF_6 pressures and at large absorbed energies. Under these conditions the V-T relaxation time becomes comparable to the typical ~200 ns input pulse duration. However, even in these circumstances the CO_2 absorptions at a given vibrational temperature are independent (to within 15%) of the rotational temperature chosen . This somewhat surprising prediction results from the fact that many vibration and rotation levels participate in the absorption at each CO_2 laser line. Raising T_R increases the rotational population for transitions which involve J-states with J above J^{max} (at 300 K, J^{max} ~48) but at the expense of the population involving low J values.*

2.4 Comparison of the Model with Experiment

Previous studies of the absorption properties of SF_6 as a function of temperature considered the case in which all the SF_6 degrees of freedom were in thermal equilibrium, characterized by a single temperature [29]. Hence, the rates at which the energy is exchanged

---

*Exceptions to this rule are the shorter wavelength CO_2 lines for which the J numbers of absorbing states are predominantly above J^{max} at 300 K. However, even in this case the absorption coefficient changes only by a factor of 5 at T_R = 1000 K with respect to the T_R = 300 K absorption, while a corresponding change in T_V produces a change of over a factor of 350. These lines are generally not of great interest due to their small low-signal absorptions at 300 K, which are reduced even further by vibrational heating. The result is that the variation in the level populations with temperature are basically determined by the vibrational Boltzmann distribution only.

between the different molecular degrees of freedom was of no importance. The application of a model such as the vibrational bath to describe the response of SF_6 to a pulse of radiation is not generally possible if the pulse is sufficiently short and/or intense that the vibrational, rotational and translational degrees of freedom can no longer reach thermal equilibrium at a single temperature. For pressures under a few hundred Torr, typical CO_2 laser pulses of $\sim$200 ns FWHM are much shorter than the V-T relaxation time (150 μs-Torr [33]). Consequently, on the time scale of such pulses, equilibrium between vibrational and translational degrees of freedom is prevented. The laser pulse energy is therefore absorbed solely into the vibrational degrees of freedom, thereby increasing the amount of energy stored in the vibrational modes. The rapidity with which this energy is redistributed determines whether thermal equilibrium is maintained within the vibrational bath for the duration of the pulse. Clearly, the vibrational temperature will not be the same as the translational-rotational temperature of the gas.

Various double-resonance experiments were performed to study the general applicability of the vibrational bath model in determining the absorption of vibrationally heated SF_6. In these experiments a high power CO_2 laser pump pulse is partially absorbed by the SF_6 and then a much lower power CO_2 laser probe is used to determine the absorption coefficient, for various frequencies, at the new vibrational temperature. The following data is taken from Taylor et al. [20] where a more complete description of the double-resonance experiments is given.

Figure 2-4 shows the transmission measurement data obtained from a double-resonance experiment performed at 50 Torr of SF_6, at a cell

Fig. 2-4

Absorption as a function of CO_2 wavenumber. The open circles represent 300 K small-signal experimetal data. The remaining data was obtained from double-resonance experiments using a P(26) pump pulse (~220 ns FWHM) at 50 Torr of SF_6, at a cell thickness of 0.16 cm and with pump input intensities of 3.8×10^4 W/cm^2 (Δ), 1.2×10^5 W/cm^2 (x), and 3.8×10^5 W/cm^2 (•). The solid curves represent the bath model predictions at 300 K, together with those at the spatially-averaged temperatures of 470 K, 800 K and 1250 K.

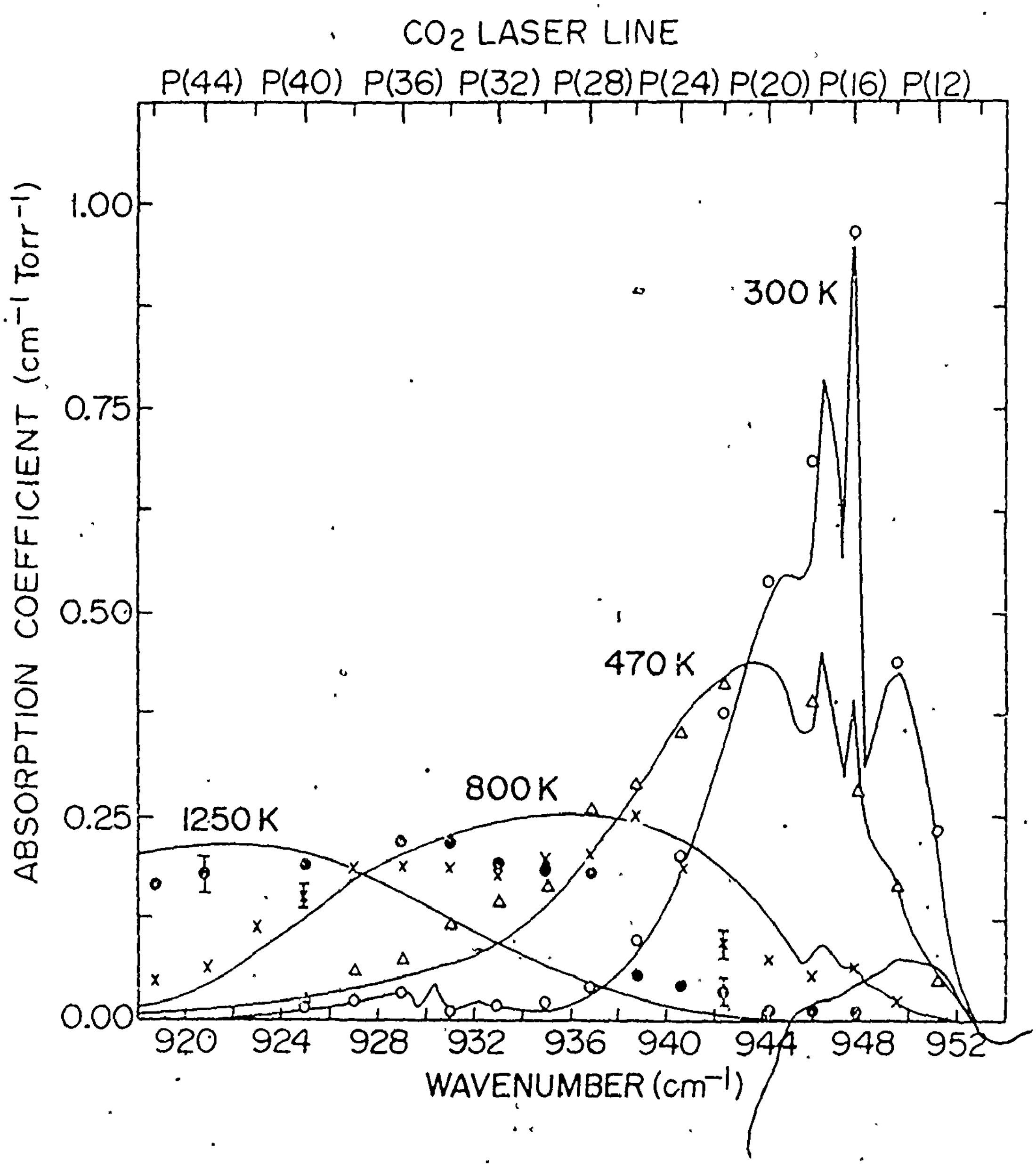
CO2 LASER LINE
P(44) P(40) P(36) P(32) P(28) P(24) P(20) P(16) P(12)
ABSORPTION COEFFICIENT (cm⁻¹ Torr⁻¹)
1.00
0.75
0.50
0.25
0.00
300 K
470 K
800 K
1250 K
920 924 928 932 936 940 944 948 952
WAVENUMBER (cm⁻¹)

thickness of 0.16 cm and with input intensities of 3.8×10^5, 1.2×10^5, and 3.8×10^4 W/cm^2, using a P(26) CO_2 laser pump pulse of ~220 ns duration (FWHM). The experimental absorption coefficients were obtained from the transmission data from the double-resonance experiments just after the laser pulse has passed through the absorber. Fig. 2-4 includes the 300 K SF_6 experimental small-signal absorption coefficients measured using a low intensity TE CO_2 laser. Also shown in this figure (as solid lines) are the absorption predictions of the bath model for the four vibrational spatially-averaged temperatures* which gave the best fit to the experimental data. In every case these temperatures were within 15% of the temperatures calculated using the experimental pump pulse transmissions, cell thickness, input intensity, pulse duration, and SF_6 gas pressure. The generally good agreement between the experimental data and the model predictions supports the assumptions made in the model. Good agreement was also found in the high temperature case (1250 K) for the P(56) CO_2 rotational line at 907.8 cm^{-1}, where both absorption coefficients are ~0.1 cm^{-1} Torr^{-1}. Such agreement at a wavelength so far removed from the band center strongly supports the general applicability of the model.

Similar experiments were performed to determine the applicability of the model to interpreting the dynamics of the absorption. In these experiments, the change in absorption was monitored at the

---

*Account was taken of the temperature gradient produced in the SF_6 gas cell by the pump pulse in determining the theoretical probe transmission. These temperatures were within 15% of the temperatures determined from the experimental measurements.

probe frequency at the *same* time as energy was being absorbed from the pump. Figure 2-5 compares P(26) pump experimental double-resonance curves, obtained with 10 Torr of SF_6 and a cell thickness of 0.25 cm, with curves generated from the absorption against temperature data of Fig. 2-2 at a temperature of 700 K. The model temperature of 700 K represents the final vibrational temperature after the pump pulse has left the gas cell, and is within 25% of the temperature calculated using pump transmission data, input intensity, pulse duration, cell thickness, and SF_6 pressure.*

The theoretical double-resonance curves were generated by calculating the energy absorbed and the temperature change for each pump-pulse increment, and then obtaining a transmission for all the CO_2 probe lines from the curves of Fig. 2-2. The P(26) curve exhibits a fast rise in transmission, followed by a steady fall to a final transmission level lower than that at 300 K. The portion of the transmission rise not accounted for by the model is attributed to intensity saturation effects of the pump on vibrational and rotational levels common only to the P(26) absorption. In these experiments the transmitted pump pulse shape was consistent with the observed double-resonance signal at that line. Note that there is very good agreement on the shapes of these curves and also that there is quite good agreement in the actual transmission values and positions of the input pump peak with respect to the double-resonance signals. The agreement is

*The temperature agreement to within 25% rather than the 15% mentioned earlier represents a decrease in the accuracy of obtaining the amount of energy absorbed in the SF_6 gas cell. This is due to the fact that the fraction of the pump energy absorbed in this case was ∿20% (compared to the ∿70% previously). Consequently, fluctuations in the transmission measurements (∿5%) can produce a 25% error in the estimated energy absorbed compared with a 15% error in the previous calculations.

Fig. 2-5

A comparison of experimental P(26) pump double-resonance curves at various CO_2 rotational lines with those predicted by the heating model. The gas pressure was 10 Torr, the cell thickness 0.25 cm, the input intensity 1.9×10^5 W/cm^2, and the pump transmission was 80%. The arrows indicate the position of the peak of the pump pulse.

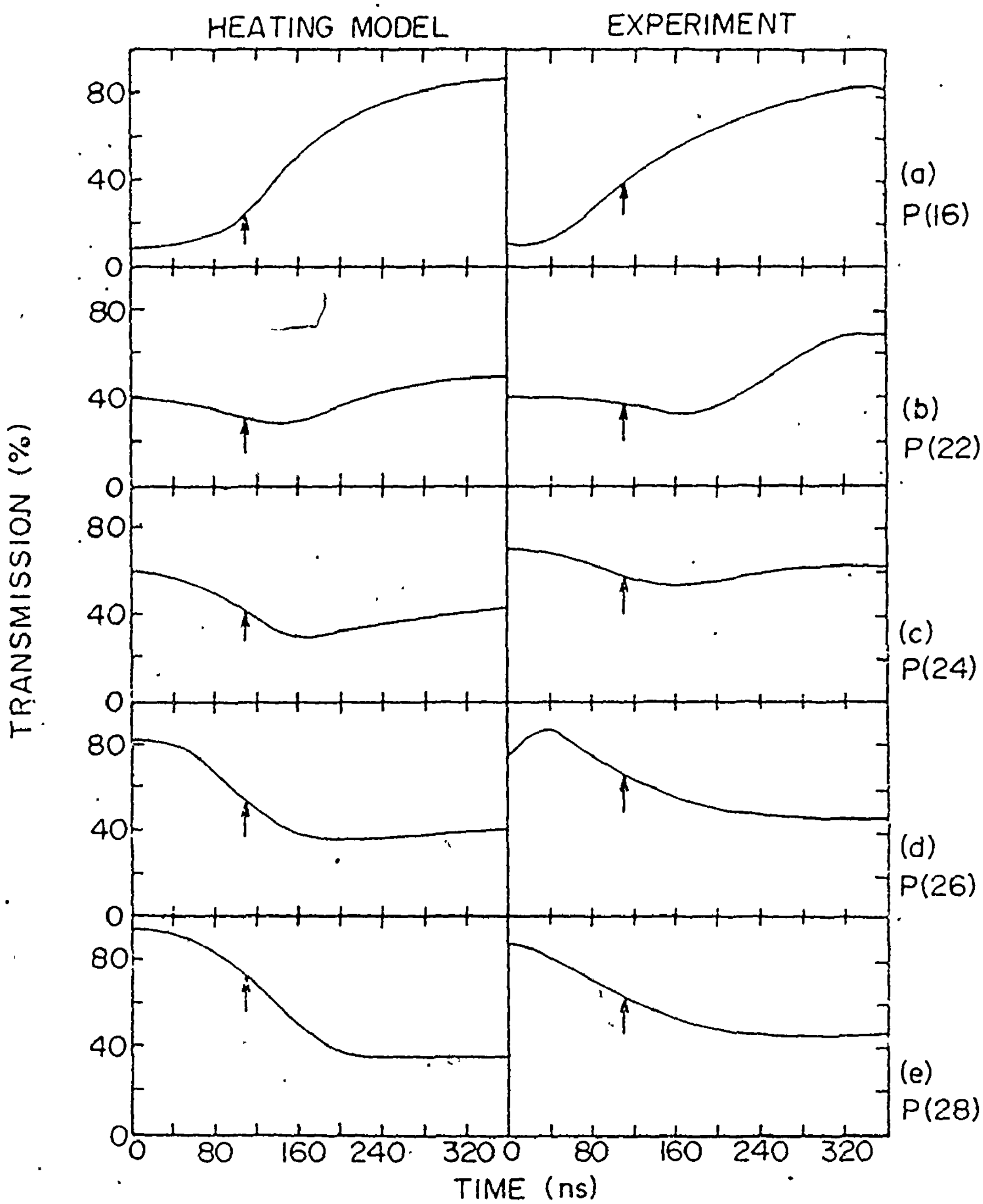

HEATING MODEL
EXPERIMENT
TRANSMISSION (%)
0
40
80
(a)
P(16)
(b)
P(22)
(c)
P(24)
(d)
P(26)
(e)
P(28)
0
80
160
240
320
TIME (ns)

remarkable when one considers that there were no adjustable parameters used in the model predictions and that the small-signal absorptions were not adjusted to agree with the experimental probe laser absorptions in the absence of the pump beam. A similar experiment at 10 Torr of SF_6 but with a P(16) pump,* also gave good agreement with the calculated transmissions and double-resonance signal shapes. Double-resonance patterns have also been observed at 1 Torr of SF_6. However, no attempt was made to obtain quantitative double-resonance data due to the small changes in transmission at this pressure.

2.5 Summary

This chapter has dealt with the development of the vibrational bath model and its application to SF_6 absorption near 10.6 μm. In particular, it has been shown that the model can also predict the dynamics of the absorption processes. This is especially significant for, at low pressures, the collisional relaxation times become long compared to the duration of the laser pulses. However, in the model it is assumed that all the vibrational and rotational levels reach equilibrium in a time short compared to the input pulse duration and that they can be characterized by a Boltzmann temperature distribution. The successful application of the vibrational bath model to these cases is due to the very rapid, collisionless, V-V relaxation processes that exist in large polyatomic molecules such as SF_6 [19].

---

*Most of the absorption on the P(16) line comes from the ground state whereas for P(26) the absorption occurs mainly at or greater than 1000 cm^{-1} above the ground state.

These very rapid energy exchange processes are due primarily to the large density of states that exist in such molecules and the subsequent coupling between them. The general applicability of the vibrational bath model to this low pressure regime is discussed in greater detail in Chapter 5.

CHAPTER 3

HIGH PRESSURE SF_6 PULSE TRANSMISSION NEAR 10.4 μm

3.1 Introduction

The SF_6 transmission characteristics obtained using a pulsed CO_2 laser operating in the 10.4 μm band have been described in detail by Garside et al. [34]. In that paper the intensity dependence of the SF_6 absorption on three CO_2 rotational lines, P(14), P(20), and P(26), (which characterize the absorption saturation behaviour of the entire 10.4 μm band), was reported for more than an order of magnitude variation in the SF_6 pressure. The saturation behaviour at these CO_2 lines was interpreted in terms of a 4-level, non-steady-state model. It was noted that good agreement was obtained between the model and the observed transmission characteristics for the P(14) line. The P(20) transmission curves could also be predicted over a large SF_6 pressure range. However, at increased SF_6 pressures, there was a small range of input intensities for which the observed transmitted pulse shape progressively broadened to durations beyond that of the input pulse. This behaviour could not be accounted for by the 4-level model. The deviation between theory and experiment becomes pro-ressively worse at longer CO_2 wavelengths (increased P values). For example, the 4-level analysis for the P(26) CO_2 line could not fully re-produce the pulse broadening observed at the transmission minima of Fig. 3-1, or the unusual shape of the 10 Torr transmission curve in that figure. It was therefore suggested that a model which incorporated the multilevel nature of the SF_6 absorption, such as the vibrational bath model described in the previous chapter, was necessary to describe fully the transmission properties of all CO_2 lines [34]. The double-resonance experiments, referred to in the previous chapter, verified that the model could account for the pump-induced SF_6 absorption dynamics over a wide range of CO_2 wavelengths and SF_6 pressures, when the pump and probe wavelengths were different. Here it is demonstrated that, at high SF_6 pressures (typically $\gtrsim$ 200 Torr), the transmission behaviour of the pump pulse itself can be entirely accounted for by the vibrational bath model without requiring the inclusion of intensity saturation effects. It is also demonstrated that at high SF_6 pressures a train of short pulses exhibits transmission behaviour consistent with the vibrational heating model. At lower SF_6 pressures, a combination of intensity saturation processes and increased pulse transmission due to vibrational heating are necessary to describe fully the absorption saturation behaviour of SF_6. This will be discussed in Chapter 5.

3.2 Application of the Model

The model assumes that all vibrational and rotational levels of SF_6 reach equilibrium in a time short compared to the input pulse duration, and that these levels can be characterized by a Boltzmann temperature distribution. As shown in Chapter 2 and Ref. [20], the results of double-resonance experiments indicate that these are very reasonable assumptions for a wide range of SF_6 pressures and laser pulse durations. Also discussed in Chapter 2 is that the absorption behaviour is relatively independent of the rotational temperature, which is therefore kept constant at 300 K. The vibrational Boltzmann temperature, however, is allowed to increase from 300 K. The increase depends on the amount of energy that is absorbed from the laser pulse for a given SF_6 pressure and gas cell thickness.

The transmission behaviour at a given CO_2 line can be calculated as follows. The input laser pulse is divided up into many small time increments (Δt) and each increment is fed into an absorber which is divided into spatial increments (Δz).* As energy is absorbed from the laser pulse, there is an increase in the vibrational temperature of each segment. An absorption coefficient appropriate to this new temperature is obtained from the absorption versus vibrational temperature curves given in Chapter 2. The above process is repeated for each successive increment until the entire pulse has passed through the absorber. This procedure allows calculation of both the shape and intensity of the transmitted pulse. The value of the temperature increase can be calculated from the expression which relates the energy (Q) added to n moles of an ideal gas in order to increase the temperature ΔT degrees at constant gas volume:

$$\Delta T = Q/nC_V^{tot}(T) \quad , \tag{3-1}$$

where $C_V^{tot}(T)$ is the total harmonic oscillator heat capacity at constant volume.** Deviations from the harmonic oscillator heat capacities can

---

* Δz was chosen such that the product of Δz and the small signal absorption coefficient α_0 was sufficiently small to ensure an optically thin absorbing medium. Typically $\Delta z\alpha_0 \sim 0.2$.

** The total heat capacity is the sum of the vibrational, rotational and translational components. At a vibrational gas temperature of 300K, the total heat capacity is 21 cal deg^{-1}.mole^{-1}, of which the vibrational contribution is 15 cal deg^{-1} mole^{-1}. The total heat capacity must be used in Eq. 3-1 at very high SF_6 pressures ($\gtrsim$400 Torr), where the vibration-to-translation (V-T) relaxation time becomes comparable to the 200 ns input pulse duration.

occur at vibrational temperatures >1300 K because of anharmonicities [22] and the onset of dissociation processes [35]. A full description of the effect of the latter on single pulse transmission is given in the next chapter.

3.3 Results and Discussion

The solid curves in Fig. 3-1 show the predicted P(26) transmission obtained using either the vibrational heat capacity or the total heat capacity in Eq. (3-1). Note that there is very little difference between the two curves since at large temperatures the vibrational contribution to the heat capacity is much larger than the rotational and translational contributions.

Good agreement is obtained between the transmission predicted by the model and the 200 Torr experimental data obtained from Garside et al. [34]. The error in the experimental transmission measurements is ~7%. The input intensities are known to better than 10% at low values and to within 15% at high values. The agreement is quite remarkable when it is considered that the only parameters used in the model were the input pulse shape, the peak pulse intensity, the cell thickness, and the gas pressure. These were all obtained from experimental measurements and no adjustable parameters were employed for the theoretical predictions.

The agreement between theory and experiment also extends to the shape of the transmitted pulse, as indicated in Fig. 3-2. For example, the approximate doubling of the input pulse duration shown in Fig. 3-2 (d) (a result which could not be predicted by the 4-level treatment) is well accounted for by the vibrational bath model. Furthermore, an analysis employing this model for the P(20) CO_2 line predicted both the magnitude

Fig. 3-1

Transmission of SF_6 as a function of input intensity at the P(26) CO_2 line. The dashed curves represent the experimental data obtained from Garside et al. [34] at 10 and 50 Torr of SF_6. The solid circles (•) denote 200 Torr data obtained from the same reference. Solid curves 1 and 2 represent the theoretical calculations employing the vibrational and total heat capacities, respectively.

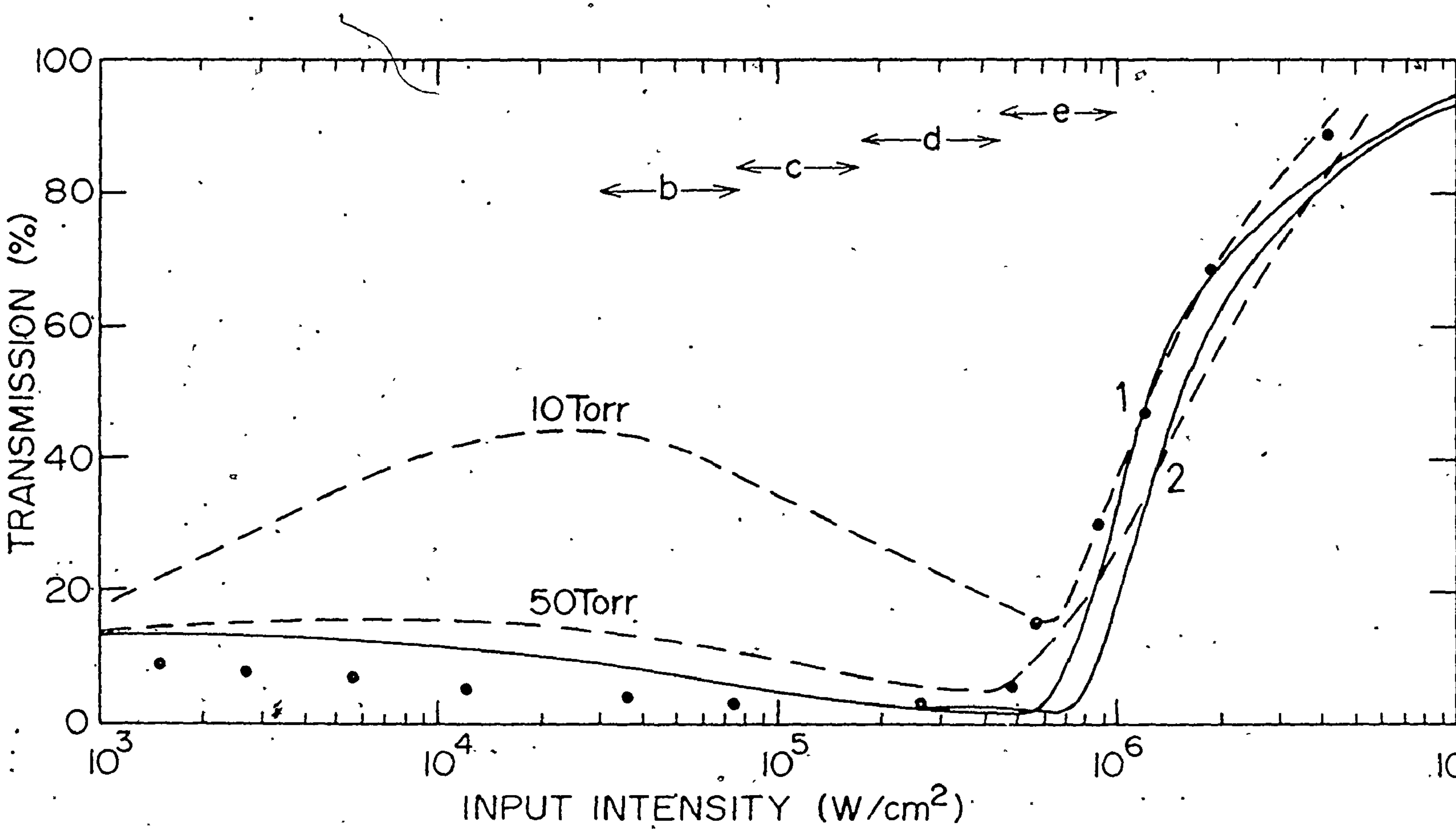
TRANSMISSION (%)
100
80
60
40
20
0
10^3
10^4
10^5
10^6
10^7
INPUT INTENSITY (W/cm^2)
b
c
d
e
10Torr
50Torr
1
2

30

Fig. 3-2

Columns I and II are the theoretical and experimental transmitted pulse shapes for the input pulse shape shown in Row (a). Rows (b) to (e) correspond to the intensity regions shown in Fig. 1. The dashed vertical lines indicate the peak of the input pulse.

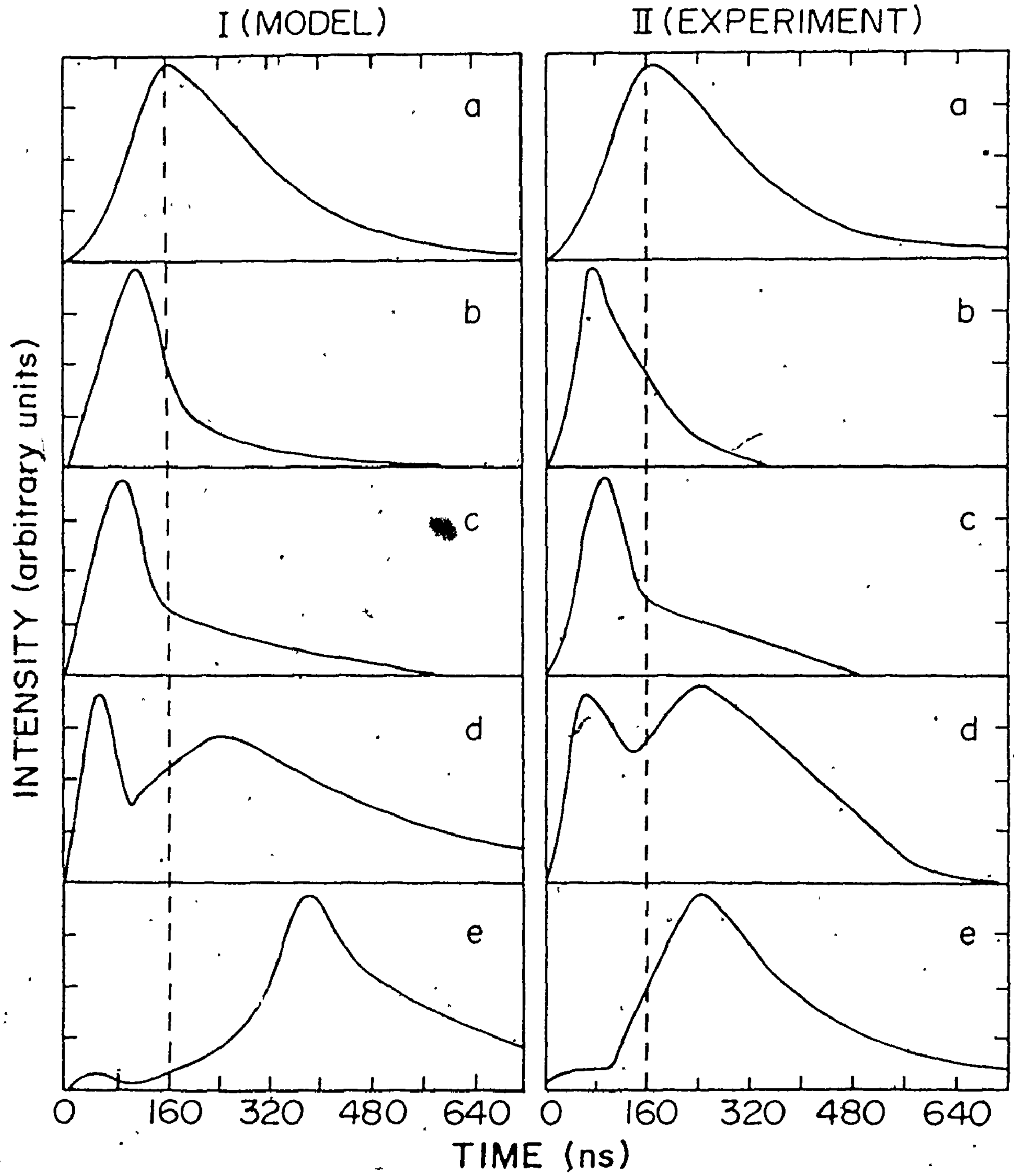

I (MODEL)
II (EXPERIMENT)
a
b
c
d
e
a
b
c
d
e
INTENSITY (arbitrary units)
0
160
320
480
640
0
160
320
480
640
TIME (ns)

of the broadening observed experimentally at high SF_6 pressures and the approximate input intensity at which pulse broadening occurred.

The model is most suitable for predicting the entire pulse transmission characteristics at high SF_6 pressures. At reduced pressures the lower coupling rate between levels allows for easier saturation of the absorption. At higher SF_6 pressures the effective level recovery times decrease, consequently making intensity saturation more difficult. However, at these higher pressures, substantial amounts of energy are coupled into the bath of levels, which can heat all the vibrational modes sufficiently to change the bath population distribution in such a manner as to change the absorption on a given CO_2 line. For the P(12)-P(18) CO_2 wavelengths, the thermal change in population at the absorbing levels results in a decrease in absorption with increasing vibrational bath temperature. At the P(24)-P(30) CO_2 wavelengths the absorption increases up to a certain vibrational temperature, reaches a maximum, and then decreases with increasing temperature.* The absorption maxima predicted for these rotational lines are shifted to higher vibrational temperatures for increasing wavelengths. This results from anharmonicities which cause the shift of absorption cross-section maxima to progressively higher energy levels at longer wavelengths. A maximum in the absorption occurs when the vibrational bath population distribution, which is also shifted to higher levels with increased vibrational temperature, is centered at the levels corresponding to the cross-section maxima. It is just the passage of the bath population distribution through regions where the P(26) line experiences a maximum

* The P(20) and P(22) lines have behaviour which lies somewhere in between the other two sets of lines and display very little change in the absorption for the first 100 K temperature rise.

absorption cross-section which accounts for the observed transmission minima in Fig. 3-1, and the observed pulse shaping on this line (Fig. 3-2). Note that even at low SF_6 pressures heating effects can substantially contribute to the overall transmission behaviour. This is evidenced by the presence of an absorption minimum in the 10 Torr P(26) transmission curve similar to that observed for high SF_6 pressures. The pulse shaping at 10 Torr is also very similar to that depicted in Fig. 3-2 for 200 Torr of SF_6.

At sufficiently high SF_6 pressures, the entire experimental transmission curves and those predicted by the model should be very similar. This is dramatically illustrated in Figs. 3-3 and 3-4 for the P(14) and P(20) CO_2 lines, respectively. The 100 Torr data in these figures shows that the agreement between the individual transmission curves (for a fixed pressure) exists for pressures greater than 100 Torr.

Pulseshaping effects can also occur when energy is absorbed from a train of $\sim$4.5 ns (FWHM) mode-locked pulses. Fig. 3-5 illustrates the strong asymmetric narrowing of the P(26) pulse train envelope after passage through 10 Torr of SF_6. This pulseshaping is similar to that observed in Fig. 3-2 (b) for a $\sim$200 ns non-mode-locked input pulse. Fig. 3-6 illustrates the transmission behaviour of mode-locked pulse trains at the P(20) CO_2 line passing through 250 Torr and 20 Torr of SF_6. The gas cell thickness for 250 Torr of SF_6 was reduced so as to give the same small signal transmission as in the 20 Torr case (calculated to be $\sim 2 \times 10^{-12}$). A time delay between the input and transmitted pulse train peaks can be observed at 250 Torr of SF_6. Furthermore, there is very little narrowing of individual mode-locked pulses (<10% of the FWHM). Similar results were obtained at low SF_6 pressures (10-20 Torr) and approximately 1 atm of air. On the

Fig. 3-3

Transmittance at the P(14) CO_2 line through a path length L in SF_6, as a function of input intensity. Experimental data, denoted by (x), (o), and (•), was obtained at SF_6 pressures of 100 Torr, 400 Torr and 760 Torr, respectively. The calculated small-signal transmittance at 760 Torr is ∿8. The dashed line represents the 100 Torr experimental data; the solid curves are the theoretical transmissions calculated using $C_v^{tot}(T)$.

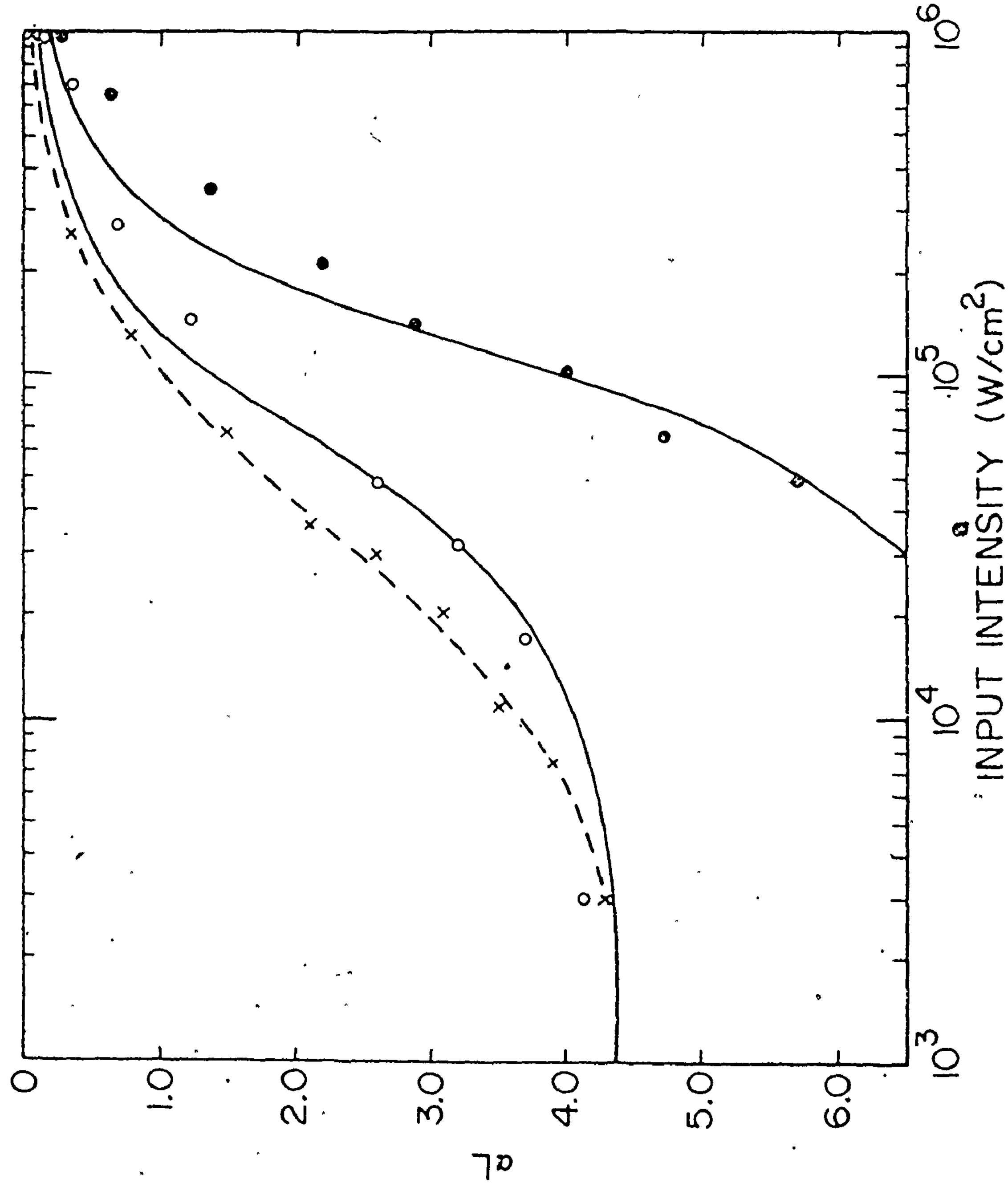

αL
0
1.0
2.0
3.0
4.0
5.0
6.0
10^3
10^4
10^5
10^6
INPUT INTENSITY (W/cm^2)

Fig. 3-4

Transmittance at the P(20) CO_2 line, through a path length L of SF_6, as a function of input intensity. Experimental data, denoted by (x), (o), and (•), was obtained at SF_6 pressures of 100 Torr, 400 Torr and 760 Torr, respectively. The calculated small-signal transmittance at 760 Torr is ~10. The dashed line represents the 100 Torr experimental data; the solid curves are the theoretical transmissions calculated using $C_v^{tot}(T)$.

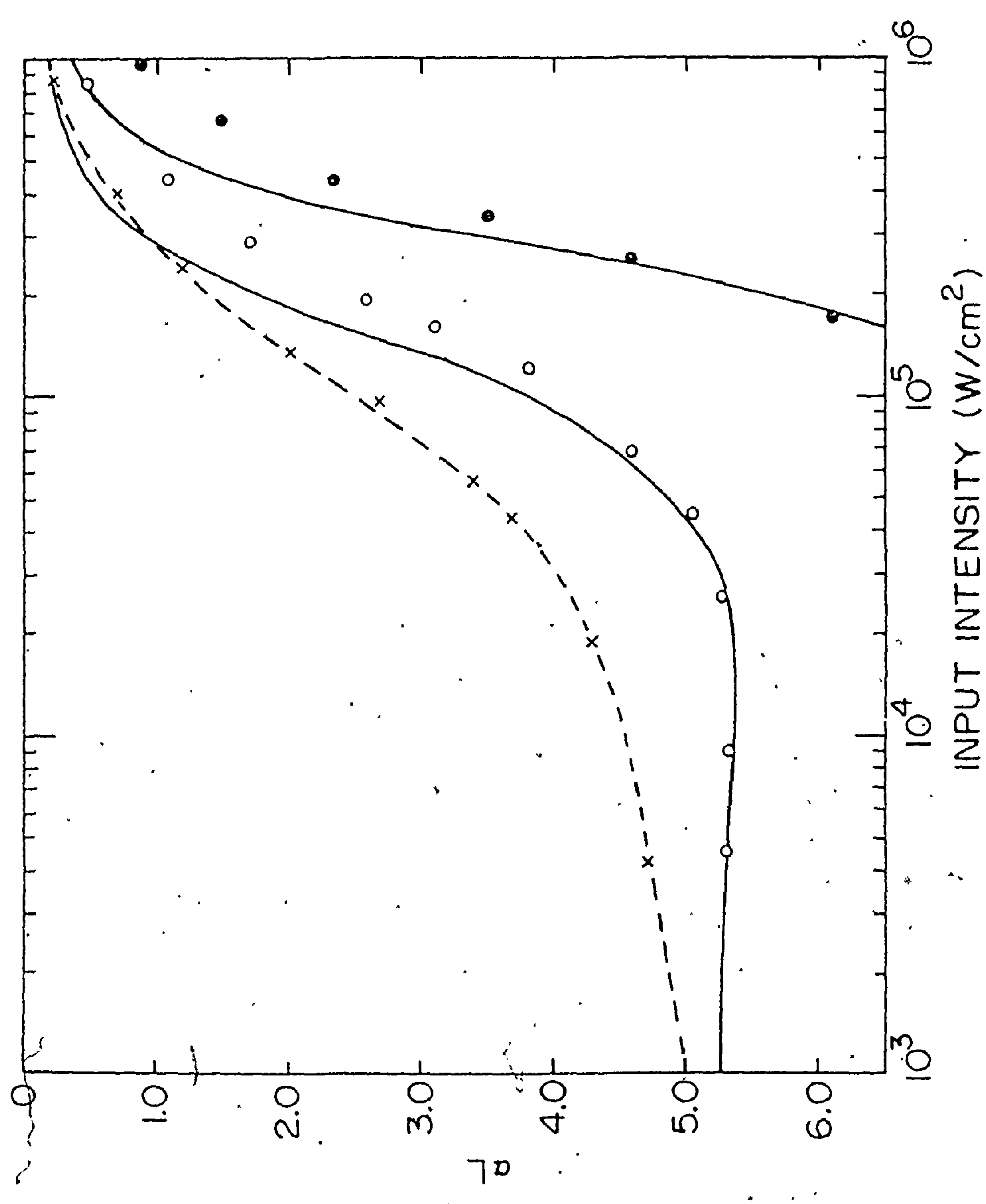

INPUT INTENSITY (W/cm²)
αL
0
1.0
2.0
3.0
4.0
5.0
6.0
10³
10⁴
10⁵
10⁶

Fig. 3-5

The top curve shows a mode-locked pulse train (at the P(26) CO_2 line) transmitted through an empty gas cell. The bottom curve represents the pulse train transmitted through the cell filled with 10 Torr of SF_6 (path length L = 2.5 cm). (From Ref. [38].)

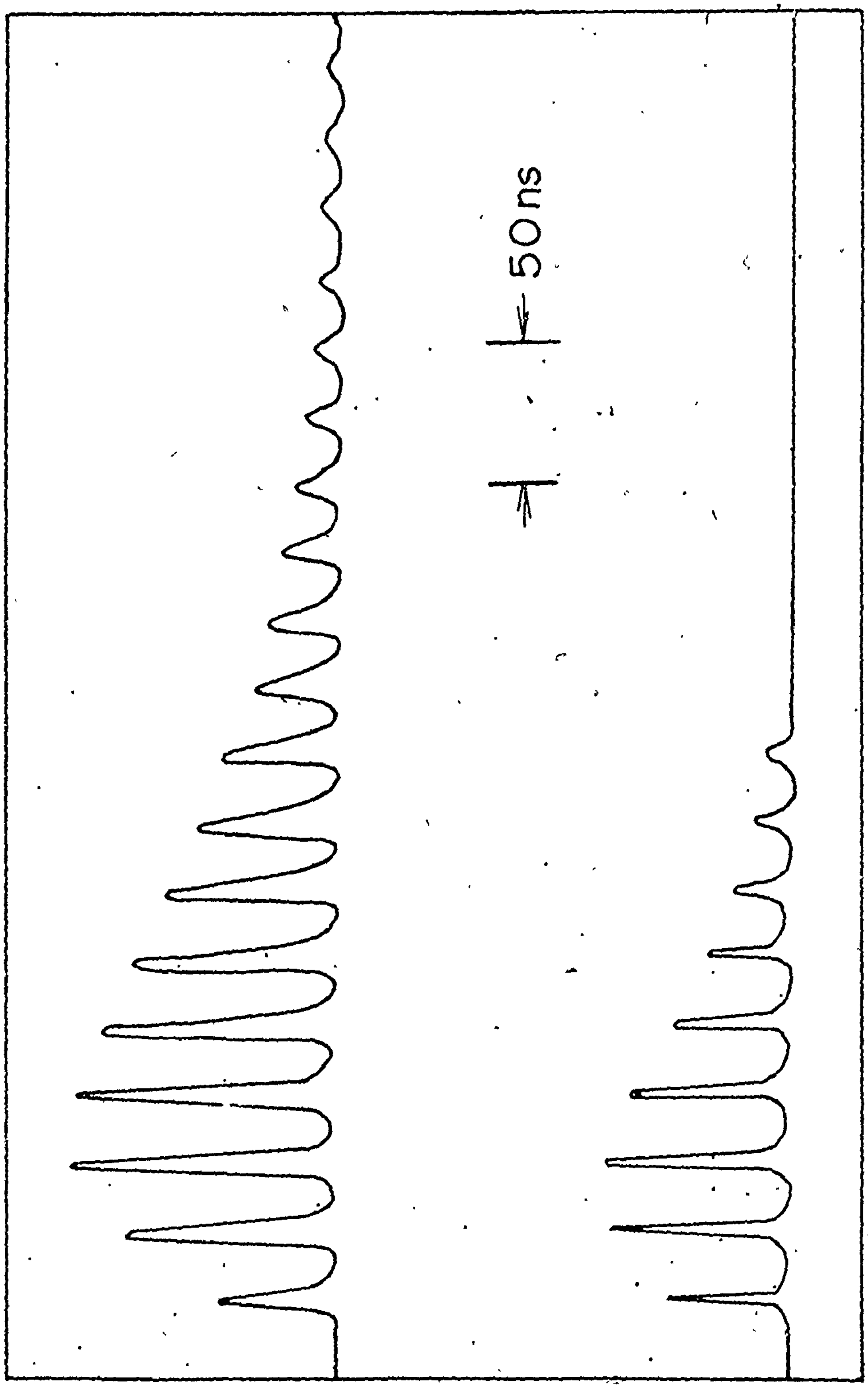
50 ns

Fig. 3-6

The top curve shows the mode-locked pulse train (at the P(20) CO_2 line) transmitted through an empty gas cell. The maximum individual pulse intensity at the cell was ~ 5 MW/cm^2. The middle and bottom curves show the transmission of the above pulse train through the cell containing SF_6 at 250 and 20 Torr, respectively. The low-signal transmission, calculated using $e^{-\alpha_0 L}$, was 2×10^{-12} for both 250 and 20 Torr. The transmissions for input pulse intensities shown in this figure were measured to be $\sim 2\%$ (referred to the peaks of the pulse trains) for both pressures. (From Ref. [38].)

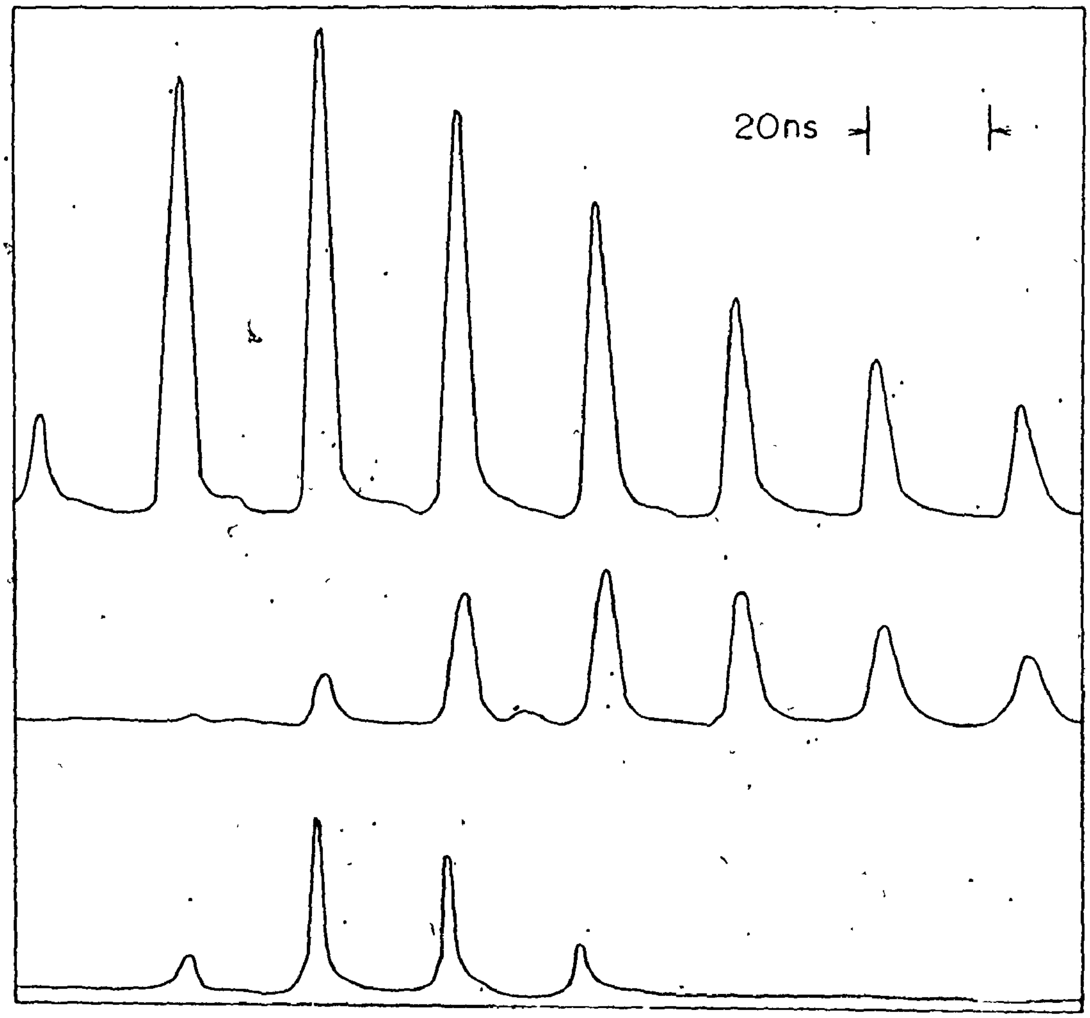
20ns

other hand, no time delay was observed for the 20 Torr SF_6 data, and substantial pulse narrowing (4.5 ns to 2 ns in the FWHM) did occur.* Similar pulse narrowing at low SF_6 pressures has been observed recently by Nowak et al. [36]. It has also been observed that adding up to 400 Torr of He to a low pressure of SF_6 (~25 Torr) narrows the mode-locked pulses (from 5 ns to ~2 ns, FWHM) [4]. Further addition of He fails to narrow the pulsewidth. Similar results were observed in Ref. [37] when using high SF_6 pressures for mode-locking a CO_2 laser. An explanation for both these observations is that, at high SF_6 and He pressures, heating effects, rather than intensity saturation effects, determine the transmission behaviour of the absorber. When this occurs the contribution of intensity saturation processes to pulse narrowing are suppressed relative to the pulse shaping effects due to vibrational heating. This latter process tends to enhance the transmission on the pulse tail and prevents pulse narrowing from occurring across the mode-locked pulse train.

At sufficiently high input intensities, vibrational anharmonicities can be compensated for by power broadening allowing multiple photon absorptions to occur up the ν_3 vibrational ladder [30]. Such an absorption process could be important in predicting the exact transmission behaviour of very high intensity (above a MW/cm^2) mode-locked pulses through SF_6. Furthermore, the onset of such a process may account for the discrepancy observed between the experimental transmissions at high input intensities (shown in Figs. 3-3 and 3-4) and those predicted by the vibrational bath model.

---

*The 2 ns may represent an upper limit since the instrumentation risetime limited the minimum detectable pulsewidth to ~2 ns [38].

3.4 Summary

It has been demonstrated that the vibrational bath model, which takes into account the complex multi-level absorption spectrum of SF_6, can predict the entire transmission behaviour of CO_2 laser pulses through high pressure SF_6. It is particularly important to note that, although the absorption is strongly "saturated" at high intensity, no genuine intensity-dependent saturation process is involved. For high P-value CO_2 rotational lines, clear evidence is found for the persistence of vibrational heating effects down to low SF_6 pressures. This is consistent with the inference made in Chapter 2, that for vibrational levels more than 1000 cm^{-1} above the ground state, very rapid vibrational energy exchange occurs even at low pressures. These exchange processes, and their effect on SF_6 pulse transmission, are discussed in greater detail in Chapter 5.

CHAPTER 4

Effect of Dissociation on SF_6 Absorption

4.1 Introduction

The transmission behaviour of CO_2 laser pulses through high pressure SF_6 has been discussed in the previous chapter. In particular, it was shown that the reduction of absorption for high input intensities was due to vibrational heating of the SF_6. For short wavelength CO_2 laser lines, such as P(14), the maximum vibrational temperature attained was ~1400 K. For CO_2 laser lines such as P(26) however, vibrational temperatures in excess of 1800 K are predicted. Shock-tube studies have determined that the dissociation threshold for SF_6 is ~1600 K [39]. Thus some dissociation is expected to occur for the longer wavelength CO_2 laser lines. It must be emphasized that the dissociation occurring here is distinct from the laser induced, coherent multiphoton dissociation observed in low pressure SF_6. This is presently an area of considerable interest and details of this process can be found in several recent review articles [40,41] and the references therein.

Experiments were performed to directly measure the amount of dissociation that occurs for the SF_6 pressures and input pulse energies used in the transmission measurements. In these experiments, a fixed volume of SF_6 was irradiated and small signal absorption measurements were used to determine the fraction of molecules dissociated. It has been demonstrated that SF_6 dissociation occurs via the process [42]

$$SF_6 + nh\nu \rightarrow SF_6^{**} \rightarrow SF_5^{*} + F \tag{4-1}$$

The SF_5^* can then further dissociate into SF_4. The asterisks indicate that the molecules are in excited states. It had been previously reported in the literature that SF_6 dissociation was an irreversible process [43]. Tal et al. [44] have recently demonstrated that the process is in fact reversible, and a scavenger gas must be used to correctly ascertain the amount of dissociation. The action of the scavenger is to prevent the reverse reaction from occurring by chemically reacting with at least one of the dissociation products. H_2 and O_2 were tested here as possible scavenger gases and H_2 was found to be the most effective, in agreement with the results of Dupré et al. [45]. Quick and Wittig [46] have shown that the operation of the H_2 scavenger is by the reaction

$$H_2 + F \rightarrow HF^* + H \tag{4-2}$$

and not by processes directly involving the excited SF_6 molecule, such as

$$SF_6^* + H_2 \rightarrow HF^* + \text{products} \quad . \tag{4-3}$$

Therefore, measurements performed employing SF_6- H_2 mixtures provide an accurate determination of the dissociation that would occur if pure SF_6 had been irradiated under similar conditions.

4.2 Experimental

The double-discharge CO_2 laser used in these experiments is described in detail in Ref. [37]. A grating was used to select the particular CO_2 rotational line. An apeture inserted into the laser cavity cavity ensured operation in the TEM_{00} mode. The laser was operated at atmospheric pressure and low N_2 concentration. The latter reduced the long pulse tails characteristic of operation at higher N_2 concentration. Typical laser output pulses had a duration of $\sim$125 ns FWHM at a peak intensity of $\sim$0.5 MW/cm^2 and a beam diameter of $\sim$8 mm. Larger intensities were obtained using a 10 in. focal length, anti-reflection coated, Ge lens. The SF_6 gas cell path length was less than a few millimeters in all cases. Consequently the beam size did not vary significantly over the cell length. The gas cell used initially had a path length of $\sim$1.5 mm and employed NaCl windows cemented to the cell body. During these initial experiments at the P(26) CO_2 laser line, the salt windows acquired an opaque coating on their inner surfaces. A discussion of this is given in the next section. Therefore it became necessary to construct a gas cell, as shown in Fig. 4-1, for which the windows could be readily removed for cleaning. In this cell, the salt windows were held in place by an aluminim clamping ring. O-rings are used to achieve a good vacuum seal. A perspex insert between the windows and the clamping rings was used to prevent window damage. Note that the valve is attached directly to the cell body; this aids in accurately determining the total volume of gas contained in the cell. This was necessary since each measurement of the dissociation yield corresponded to irradiation of the entire gas volume once.

High purity SF_6 and H_2 were used (obtained from Matheson) in the ratio of 1:2 and at a total pressure of $\sim$600 Torr. It was determined experimentally that no change occurred in either the dissociation yield

Fig. 4-1

Photograph of the gas cell used in the dissociation experiments. The path length in the cell is 3.8 mm and the total volume is 4.8 cm^3.

or the products formed upon addition of more H_2. The number of SF_6 molecules present before and after irradiation of the cell was determined from small signal absorption measurements employing low-power pulses from a pin-type helical CO_2 laser [47]. Infrared spectra of the products formed as a result of the dissociation were obtained using an IR spectrometer (Perkin Elmer 283) having a spectral resolution ranging from 2-7 cm^{-1}. These spectra were taken immediately after irradiation by the CO_2 laser pulses. No change was observed when the measurements were repeated on the same samples after a 24 hour period.

4.3 Results and Discussion

Figure 4-2 shows the fractional dissociation of SF_6 observed for various input energies on the P(28) CO_2 laser line. The P(28) transmission curves are very similar to those for P(26) (Fig. 3-1) except for a shift to slightly higher input intensities. The larger values of the input energy fluxes in Fig. 4-2 correspond to the region where heating effects cause the absorption to be greatly reduced. ($\sim$100 % transmission at an input energy of 9.5 J/cm^2). Figure 4-3 illustrates the fractional dissociation observed as a function of the average number of photons absorbed by each molecule of SF_6. To within experimental error, the results indicate that the dissociation yield is dependent only on the energy that is absorbed and does not depend on the CO_2 laser wavelength used. This is quite different from the strong frequency dependence observed in the coherent multiphoton dissociation of SF_6 at low pressures [48]. The slight shift of the P(26) data points

Fig. 4-2

Fraction of SF_6 molecules dissociated as a function of input energy at the P(28) CO_2 laser line. Pulse durations were $\sim$125 ns FWHM. The initial SF_6 pressure was 200 Torr, corresponding to a small signal transmission of $\sim$3%.

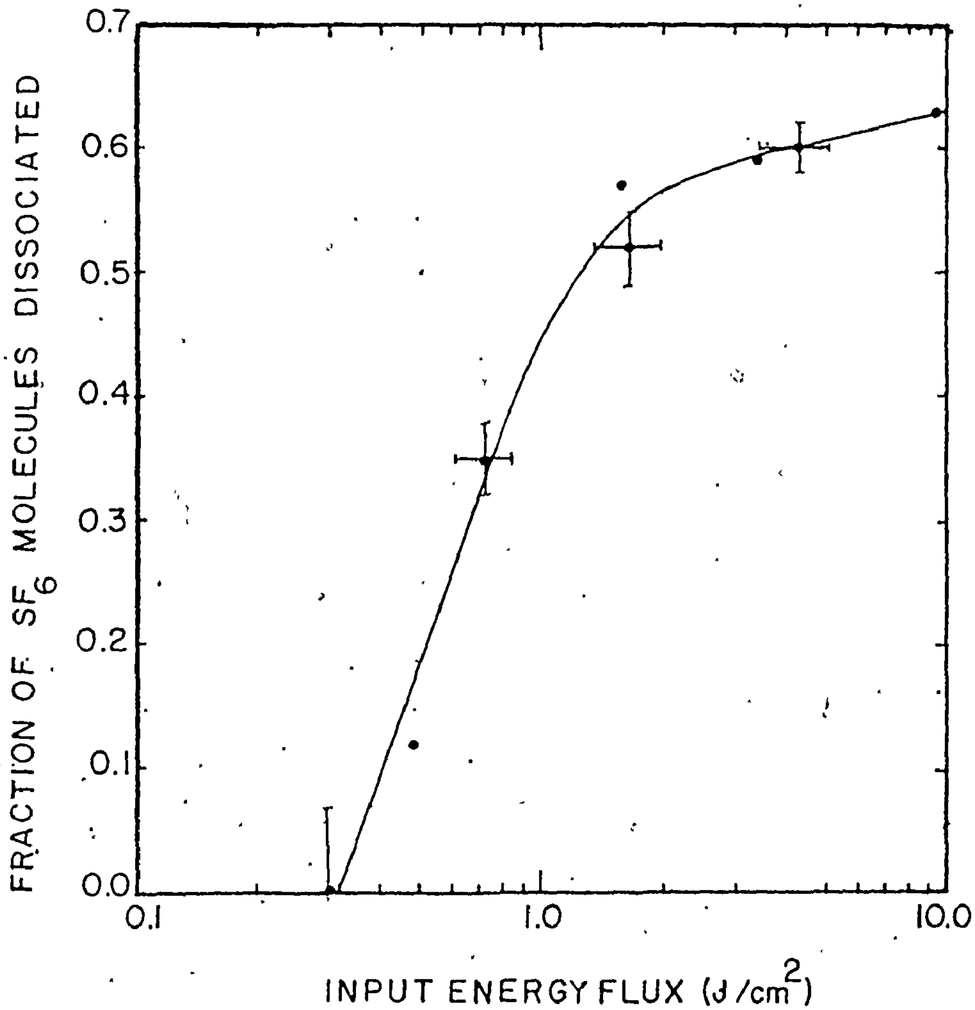
FRACTION OF SF_6 MOLECULES DISSOCIATED
0.7
0.6
0.5
0.4
0.3
0.2
0.1
0.0
0.1
1.0
10.0
INPUT ENERGY FLUX (J/cm^2)

Fig. 4-3

Fraction of SF_6 molecules dissociated as a function of the average number of photons absorbed per molecule of SF_6. Results for both the P(28) (x), and P(26) (●), CO_2 laser lines are shown.

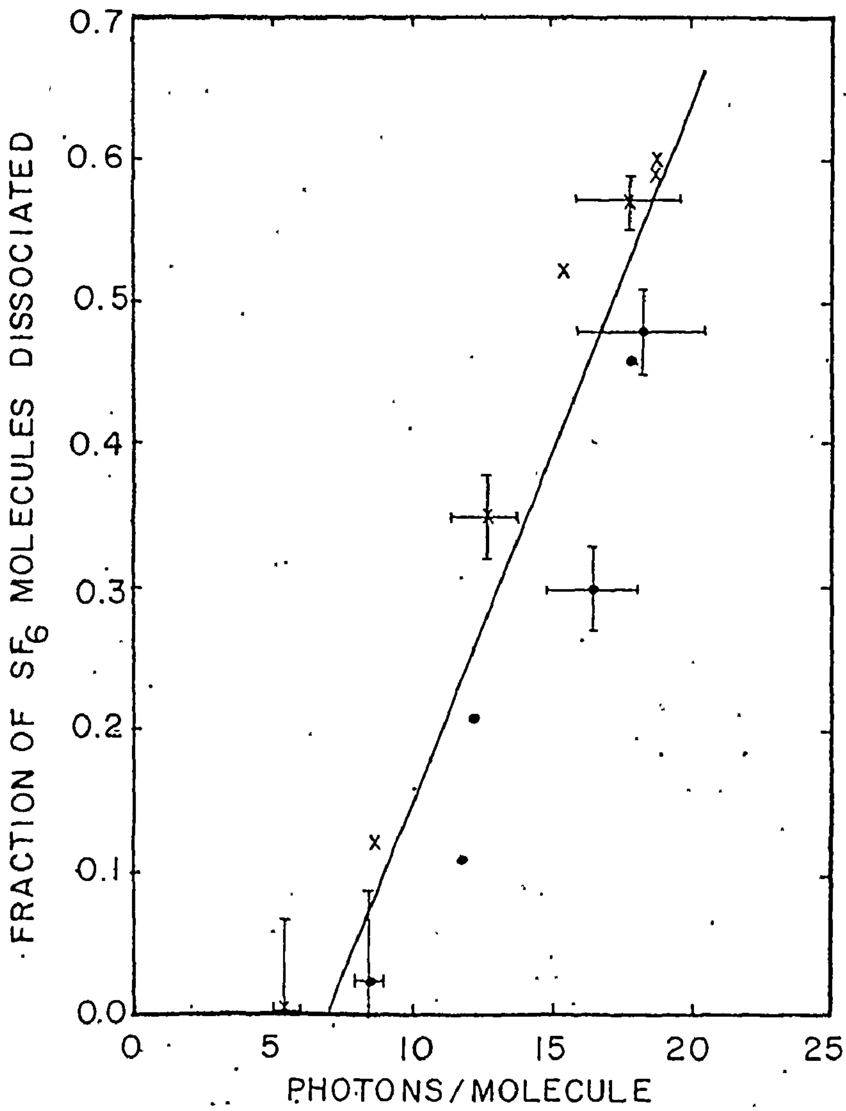

FRACTION OF SF6 MOLECULES DISSOCIATED
0.0
0.1
0.2
0.3
0.4
0.5
0.6
0.7
0
5
10
15
20
25
PHOTONS/MOLECULE

is attributed to the increasing amount of deposits on the gas cell window. In Section 4.4 it is shown that the fractional dissociation observed is in good agreement with the predictions of the vibrational bath model.

Figure 4-4 shows a comparison of the IR spectrum of pure SF_6 with the spectrum obtained when the same amount of SF_6 is mixed with H_2 and irradiated by high power CO_2 laser pulses. It was observed experimentally that when pure SF_6 was irradiated, absorption peaks corresponding to the following substances occurred:

SF_4 at 728, 867 and 889 cm^{-1} [49],

S_2F_{10} at 819, 880 and 930 cm^{-1} [49], and

S_2F_2 at 745 and 810 cm^{-1} [49].

However, Fig. 4-4(b) indicates that for SF_6- H_2 mixtures only those due to S_2F_2 remain. This suggests that the S_2F_{10} and SF_4 produced react with the H_2 molecules. A more important process in such mixtures is the formation of HF, of which the P-branch absorption spectrum is observed near 4000 cm^{-1}. Previous studies have reported visible luminescence, in the form of a pale blue light, that is associated with the infrared photodissociation of polyatomic molecules such as SF_6 [50,51]. This is readily observed in the experiments performed here as well.

The most notable features of the spectrum shown in Fig. 4-4(b) are the broad peaks occurring between 1200 and 2200 cm^{-1}. These were due to $NaHF_2$ formed by HF molecules attacking the NaCl windows [52]. The resulting light grey substance was noted in all experiments performed with the SF_6- H_2 mixtures. The window attack was not localized to the exact irradiation region of the cell, but covered a much larger

Fig. 4-4

Infrared spectra illustrating the products formed in the dissociation of high pressure SF_6. Figure 4-4(a) corresponds to 200 Torr of SF_6 at a path length of 3.8 mm. Figure 4-4(b) shows the results of irradiating the same amount of SF_6, in the presence of 400 Torr of H_2, with P(28) CO_2 laser pulses of ∿4.5 Joules/cm^2. The transmission of the pulses is ∿80%.

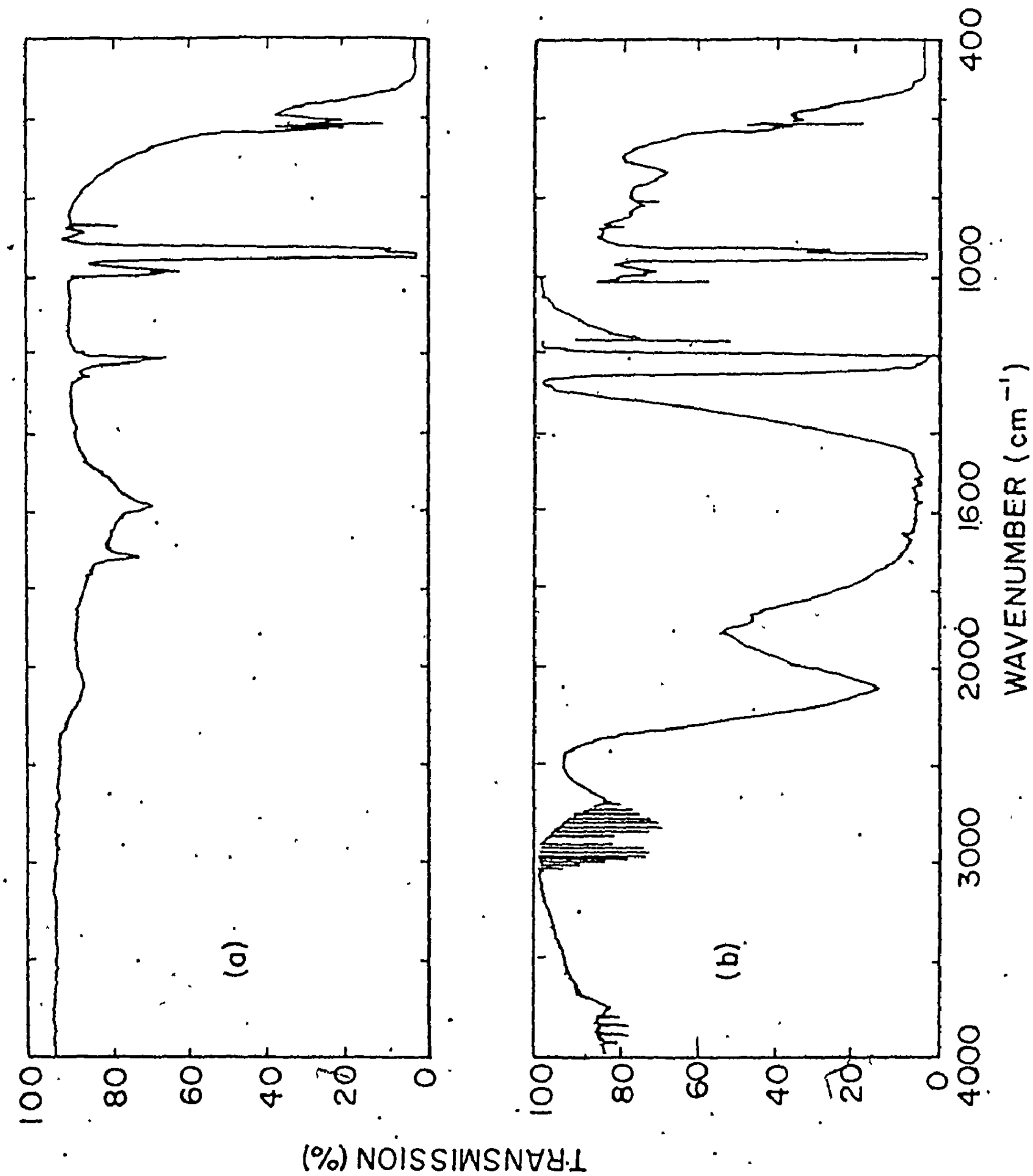
(a)
(b)
TRANSMISSION (%)
WAVENUMBER (cm⁻¹)
100
80
60
40
20
0
4000
3000
2000
1600
1000
400

area (having a diameter 3-4 times the beam diameter). The displaced chlorine atoms react to form HCl, as can be seen from its distinctive rotational spectra at 2890 cm^{-1} [53]. Dupré et al. [45] have reported reactions between quartz cell walls and the dissociation products of SF_6 to produce SiF_4 and SOF_2. The formation of $NaHF_2$ and HCl in SF_6 laser induced dissociation experiments, however, has not been previously reported. The reason for this is the entirely different nature of the present experiments. In multiphoton dissociation experiments, low gas pressures (typically <1 Torr) are contained in long absorption cells. Consequently, only a small fraction of the molecules are able to react with the salt windows at either end. In the present experiments the gas cells had very small path lengths, and thus a large percentage of the total exposed surface area consisted of the NaCl windows. Also, work on other polyatomic molecules has shown that the particular dissociation products formed can be very dependent upon the cleanliness of the windows [54]. This again illustrates the advantages of a gas cell design which permits easy removal and cleaning of the windows.

4.4 Effect of Dissociation on Single Pulse Transmission

Although it has been shown that the vibrational bath model can successfully predict the transmission of CO_2 laser pulses through SF_6, some inconsistencies remain. For P(26) pulse transmission (Fig. 3-1), the absorption of the high intensity pulses can produce vibrational temperatures in excess of 2500 K if harmonic oscillator heat capacities are used. However, the thermal dissociation threshold of

SF_6 is 1600 K [39]. Frie [35] calculated corrections to the harmonic oscillator heat capacities to allow for the onset of dissociation. Values for these corrections were incorporated into the model and provided a reduction in the vibrational temperatures. However, no proper estimate could be made of the amount of dissociation that occurs. Experiments described earlier in the chapter have demonstrated that the onset of dissociation occurs when the number of photons absorbed per molecule, <n>, exceeds $\sim$7. Substantial dissociation was observed for <n> $\approx$ 18. Recent work on multiphoton dissociation has provided considerable information on the processes that occur. The effects of these processes on single pulse transmission can be predicted by the vibrational bath model,

The dissociation limit for SF_6 occurs at $\sim$26,000 cm^{-1} ($\sim$28 CO_2 laser photons) [55]. Furthermore, Grant et al. [42] have shown that the rate of dissociation has a sharp dependence on the degree of vibrational excitation. When more than 8-9 photons in excess of the dissociation limit are absorbed, the lifetime of the excited SF_6 molecule becomes less than 1 ns. For calculational simplicity, it can be assumed that all SF_6 molecules with vibrational energies in excess of 34,000 cm^{-1} dissociate in a time short compared to the duration of a CO_2 laser pulse. Thus, for any vibrational temperature produced during the absorption of such a laser pulse, dissociation of the SF_6 continues until the vibrational temperature is reduced and no significant fraction of molecules remain above the 34,000 cm^{-1} limit. This decrease in the vibrational temperature is due to the dissociating molecules removing energy (the equivalent of 36 photons) in excess of the average amount of vibrational energy per molecule.

Figure 4-5 shows the results of incorporating the effect of dissociation into the vibrational bath model. The dashed curve represents the previous calculation described in Section 3.2. Large amounts of dissociation have minimal effect on the transmission curve because most of this dissociation occurs on the pulse tail. For example, at 5 MW/cm^2, less than 5% of the molecules dissociate before the pulse peak, yet ∿30% are dissociated over the entire pulse. However, in situations for which substantial absorption can occur at high vibrational temperatures (such as the high J-value CO_2 laser lines - see Fig. 2-2), considerable dissociation can occur in the early portions of the pulse; this will greatly effect transmission of the remainder of the pulse. In the P(26) case the pulse shaping is only slightly affected by the onset of dissociation. Even on the tail of the pulse, the decrease in the number of SF_6 molecules is offset by the reduction in vibrational temperatures and the corresponding increase in absorption.

The calculated vibrational temperatures rarely exceed 1800 K for all of the input intensities studied. After the entire pulse had passed the final temperature was ∿1500 K. This is certainly more realistic than the very high vibrational temperatures predicted if only the harmonic oscillator heat capacities are used without allowing for dissociation.

The vibrational bath model also gives an estimate of the fractional dissociation occurring. For a value $\langle n \rangle \approx 18$, which corresponds to an average vibrational temperature of ∿1700 K, the model

Fig. 4-5

Transmission of SF_6 as a function of input intensity at the P(26) CO_2 laser line. The data is taken from Ballik et al. [38]. The dashed curve represents the vibrational bath model calculations described in Chapter 3. The solid curve corresponds to similar calculations in which the effect of dissociation has been explicitly included.

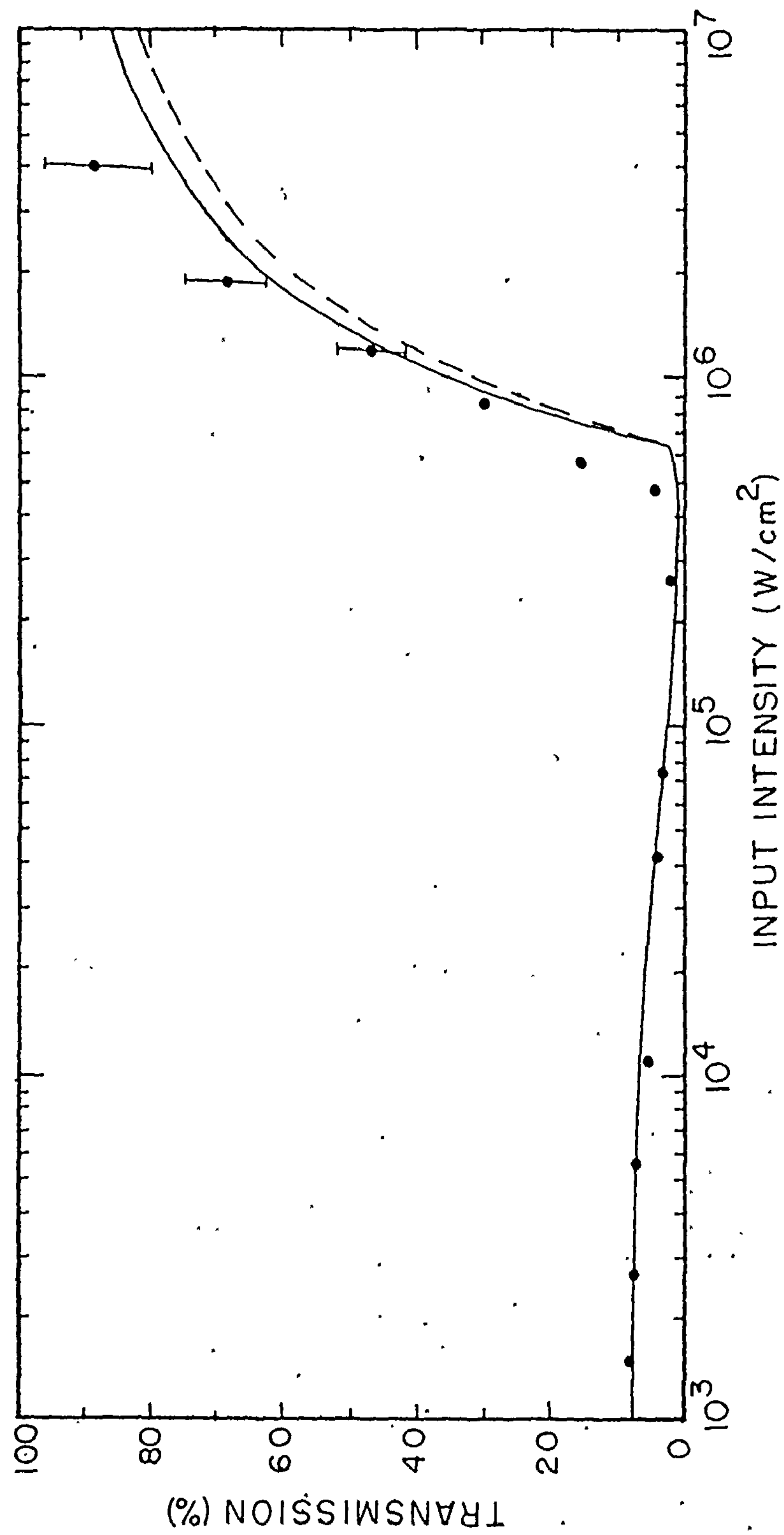

TRANSMISSION (%)
100
80
60
40
20
0
10^3
10^4
10^5
10^6
10^7
INPUT INTENSITY (W/cm^2)

predicts that $\sim$35% of the SF_6 molecules dissociate. This is in reasonable agreement with the measurements depicted in Fig. 4-3, especially when it is considered that the model does not include dissociation that occurs after the laser pulse has passed. The model predictions for both the fractional dissociation and the effect on the transmission curves are only weakly dependent upon the exact values used for the dissociation limit, and for the number of excess photons absorbed beyond this. This is again due to the opposing effects of the amount of dissociation occurring and the corresponding reduction in vibrational temperature. The best agreement between the model, the transmission data of Fig. 4-5, and the fractional dissociation of Fig. 4-3, does in fact occur when $\sim$34,000 cm^{-1} of vibrational energy are required for an SF_6 molecule to dissociate on a sub-ns timescale.

4.5 Summary

It is demonstrated that dissociation effects can be observed in the interaction of high pressure SF_6 with high power CO_2 laser pulses. The fractional dissociation can become significant once the average number of photons absorbed per molecule of SF_6 exceeds $\sim$18, corresponding to vibrational temperatures of $\sim$1700 K. The dissociation observed can be accounted for by incorporating into the vibrational bath model the dependence of dissociation rates upon the degree of vibrational excitation. It is shown that even substantial dissociation can have minimal effect on the transmission of CO_2 laser pulses through high pressure SF_6 if most of the dissociation occurs on the pulse tail.

CHAPTER 5

LOW PRESSURE SF_6 PULSE TRANSMISSION

5.1 Introduction

In Chapter 3 it is shown that the vibrational bath model can predict the transmission behaviour of CO_2 pulses through high pressure SF_6. In this high pressure regime there are no saturation effects and the absorption properties can be described completely in terms of vibrational heating. It has been reported by Garside et al. [34] that, at low pressure, true intensity saturation is plainly evident. The pressures at which these saturation effects become dominant is found to have a marked dependence on the CO_2 wavelength. Changes in absorption due to vibrational heating effects are observed even at pressures as low as 10 Torr for long wavelength CO_2 lines such as P(26). This accounts for the inability of early models, based solely on intensity saturation effects, to predict the transmission behaviour observed in such cases. Due to vibrational heating, the levels from which absorption occurs changes dramatically with the amount of energy absorbed; there is a corresponding change in the absorption cross-sections and relaxation rates. The changes in the cross-sections are discussed in Section 2.3. The emphasis in this chapter is on the investigation of the dependence of relaxation rates on the vibrational energy.

5.2 Vibration-to-Vibration Relaxation Rates

A wide range of vibration-to-vibration (V-V) energy exchange times for SF_6 have been reported in the literature and are summarized in

Table 5-1. Taylor et al. [20] suggested that the principle reason for these variations is that different regions in the vibrational bath have very different V-V relaxation rates. For example, Bates et al. [33] indicate that their observed V-V rates may be controlled by the energy transfer processes between the v = 1, ν_3 (948 cm^{-1}) and v = 1, ν_6 (346 cm^{-1}) vibrational levels. However, only a small percentage of the absorption (at only a few short wavelength CO_2 lines) occurs in this region, as can be seen from Fig. 2-3. Hence the V-V relaxation rates of Bates et al. [33] may simply be inappropriate for describing the transfer times between the levels that absorb CO_2 radiation. Further experimental evidence of the vibrational energy dependence of the V-V rates is given by Taylor et al. [20], as shown in Table 5-1. The V-V relaxation times (<20 ns-Torr) of the P(24)-P(30) lines (absorption predominantly from levels above 1500 cm^{-1}) are very different from the 150 ns-Torr relaxation time of lines such as P(14) and P(16) (absorption predominantly from vibrational levels below 1500 cm^{-1}). The reason for this may be the high density of states above 1500 cm^{-1} and the subsequent coupling that exists between these states. Recent work on coherent multiphoton dissociation has suggested that this can lead to extremely rapid, collisionless, energy exchange processes in highly excited molecules [55].

The dependence of the V-V relaxation rates on the vibrational energy is consistent with the low pressure transmission results at the P(26) CO_2 laser line, as shown in Fig. 3-1. At a pressure of 10 Torr, intensity saturation is dominant for moderate input intensities (the ascending portion of the transmission curve). However, even small

TABLE 5-1

Vibration-to-vibration (V-V) relaxation times observed in SF_6.

Observed V-V relaxation time (ns-Torr)	Method	Reference
1100	16 μm fluorescence measurements	Bates et al. [33]
300	IR double-resonance	Steinfeld et al. [56]
0.3	"	Frankel [19]
150, P(14) - P(16)	"	Taylor et al. [20]
<20, P(24) - P(30)		
3000*	"	Deutsch and Brueck [57]

*collisionless relaxation only

amounts of vibrational heating (e.g., $\Delta T_V \approx 100$ K) can shift populations to regions higher in the bath, where faster V-V relaxation rates are encountered. Hence intensity saturation becomes increasingly more difficult. Upon further vibrational heating, these changes in the V-V relaxation rates become so great that the transmission is reduced and eventually reaches the limit where only heating effects occur. This is evidenced by the similar high transmissions achieved for large input intensities at all the SF_6 pressures employed.

The dependence of the vibrational relaxation rates on the vibrational energy was investigated by transmission measurements of low pressure SF_6 in a heated gas cell. Subsequent modifications were made to the vibrational bath model to include the saturation processes. These modifications, and the application of the model to low pressure single pulse transmission, are discussed in Section 5.5.

5.3 Experimental

A helical TE CO_2 laser was used as a probe because of its excellent short and long term pulse-to-pulse reproductibility [47]. The laser was operated with high He content and with a total gas pressure of 400 Torr. Typical output pulse durations were ~200 ns FWHM. A grating was employed to select the desired rotational line. An aperture, placed inside the resonator, ensured operation in the TEM_{00} mode. The incident intensity could be varied over 5 decades by the use of attenuators (polyethylene sheets and partially transmitting mirrors) and long focal length (10 in. and 20 in.) Ge lenses. Absolute intensities were measured with a calibrated photon-drag detector. A portion of the incident beam was split-off by a NaCl flat inserted into the beam path and focussed onto an Au:Ge detector. The resulting signal was used to trigger the detection system.

Figure 5-1 shows the gas cell used in these experiments. The outer cell body is fitted with two moveable inner components which allow adjustment of the path length. The adjustable cell makes it possible to maintain a constant small-signal transmission. The moveable components are fitted with NaCl windows held in place with teflon support rings. Viton O-rings provide a vacuum seal.

Commercial heating tape (not shown in Fig. 5-1) is employed to heat the gas cell. Temperature measurements are made using an iron-constantan thermocouple inserted into the cell. After the cell temperature was allowed to equilibrate, the temperature remained constant in time to better than 5 K. It was determined experimentally that neither important temperature differences nor significant thermal gradients existed within the cell.

High purity grade SF_6 was employed (obtained from Matheson) and no further purification was attempted.

5.4 Results and Discussion

Figure 5-2 shows the results of transmission measurements, taken at different temperatures, for the P(14) CO_2 laser line. The P(14) absorptions occur from low lying vibrational levels for all vibrational temperatures encountered here. The differences in the saturation behaviour can be accounted for by the increase in the collisional V-V relaxation rates. As the SF_6 is heated, at constant volume, there is a change in the V-V relaxation rates due to the increase in pressure. It has

Fig. 5-1

Photograph of the gas cell. The moveable inner components allow the path length to be adjusted from 1.5 cm to 8 cm.

Fig. 5-2

Transmission of SF_6 as a function of input intensity at the P(14) CO_2 line. The SF_6 pressure at 300 K is 5 Torr. The data corresponds to initial temperatures of 300 K (x), 350 K (●), and 400 K (▲). The dashed curve represents the predictions of the bath model, in the absence of saturation, at 400 K.

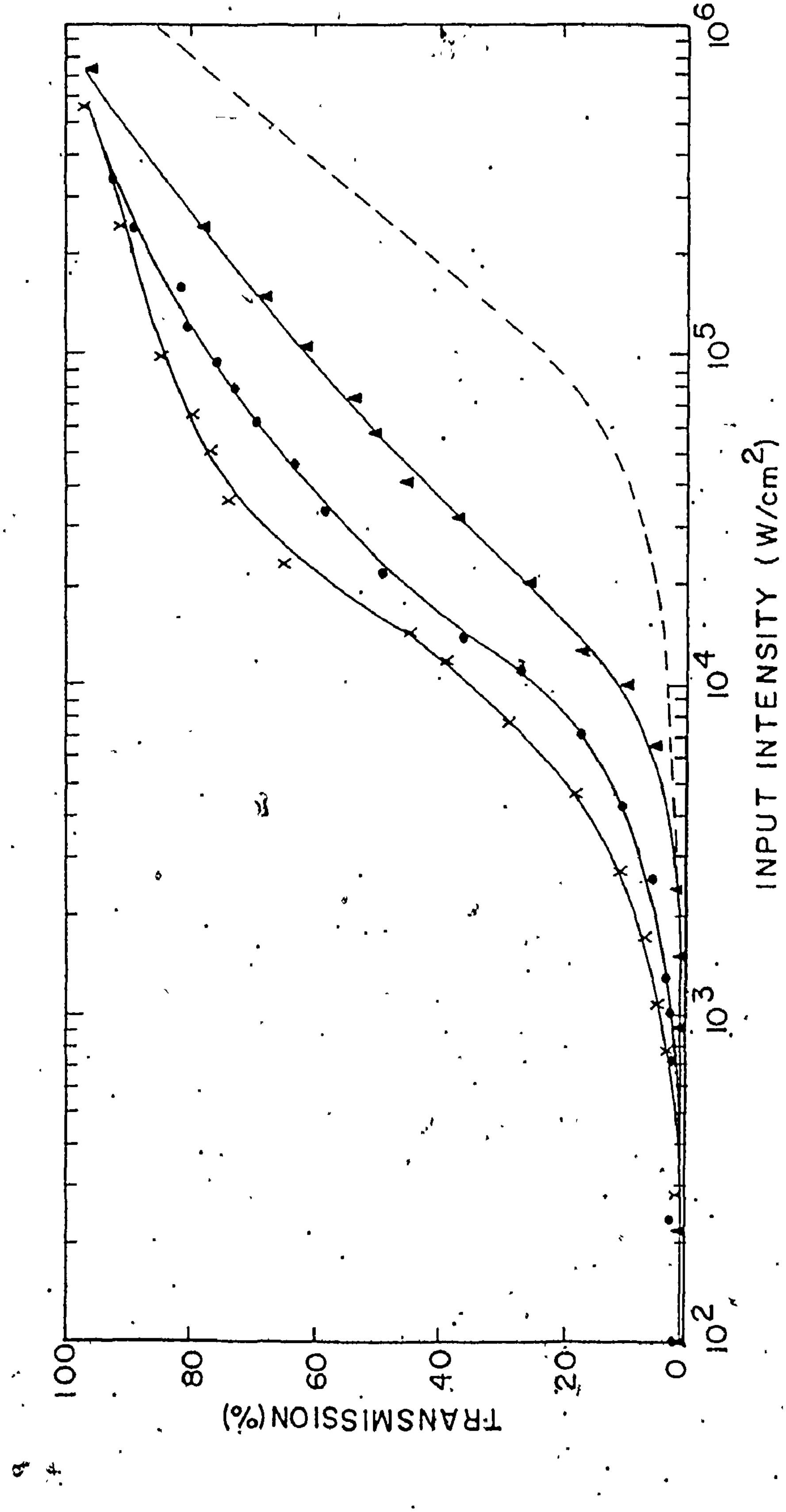
TRANSMISSION (%)
100
80
60
40
20
0
10²
10³
10⁴
10⁵
10⁶
INPUT INTENSITY (W/cm²)

recently been shown that the collisonal cross-sections for SF_6 molecules increase with the degree of vibrational excitation [57]. It has been pointed out above that the vibrational bath model predicts that there is no significant P(14) absorption occurring from levels above 1500 cm^{-1}. This is the region in which collisionless V-V rates become important. Cantrell and Galbraith [58] have calculated that anharmonic splittings of the vibrational levels allow coherent multiphoton absorption up the vibrational "ladder" for lines such as P(14). The contributions to the total absorption from regions of rapid energy transfer would lead to an increase in the overall vibrational relaxation rate. The dashed curve in Fig. 5-2 represents the vibrational bath model predictions, in the absence of intensity saturation, for a temperature of 400 K. Although the degree of saturation can be reduced by heating of the SF_6, it is evident that significant saturation persists.

Figure 5-3 gives the results of similar experiments performed at the P(24) CO_2 laser line. The effects of heating on SF_6 absorption are much more distinct and can be readily interpreted in terms of shifts in the vibrational populations to regions where the density of states is much higher. Consequently, there is more rapid energy exchange. At 300 K, ~45% of the P(24) absorption occurs from levels under 1000 cm^{-1} and less than 20% from above 1500 cm^{-1}. At 350 K, approximately one third of the absorption occurs from each region. The sharp reduction in the saturation at 400 K is due to reduced absorption from below 1000 cm^{-1} (~20%) and increased absorption (50%) from above 1500 cm^{-1}: At 450 K, the contributions from these regions become 15% and 60%, respectively. The shift in the transmission curves to lower intensities with increasing

Fig. 5-3

Transmission of SF_6 as a function of input intensity at the P(24) CO_2 line. The SF_6 pressure at 300 K is 5 Torr. The data corresponds to initial temperatures of 300 K (x), 350 K (●), 400 K (▲) and 450 K (o).

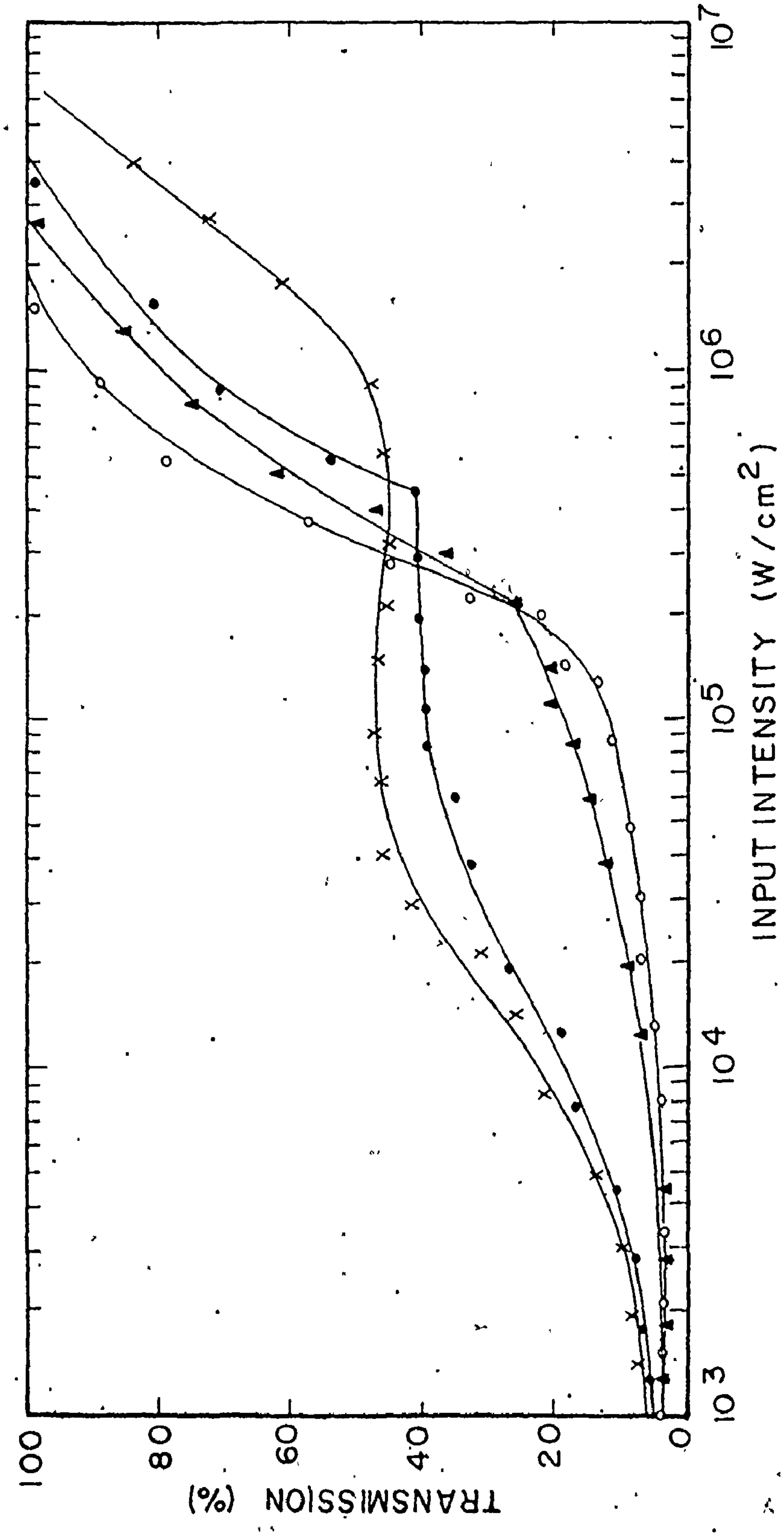
TRANSMISSION (%)
100
80
60
40
20
0
INPUT INTENSITY (W/cm^2)
10^3
10^4
10^5
10^6
10^7

temperature corresponds to less additional vibrational heating being required to achieve the temperatures for which the absorption begins to decrease rapidly.

The bath model is able to predict the pulse shaping observed throughout these experiments. For example, the dependence of absorption on temperature is such that the effect of vibrational heating for P(24) at 450 K is similar to that for P(20) at 300 K. This is shown by the pulse broadening which is observed in both cases for moderate transmissions. Similarly, the 300 K P(24) case is very similar to that of P(26) at 350 K. The most apparent effect is the disappearance of pulse break-up (Fig. 3-2(d)) which would occur just before the rapid rise to high transmittances. The disappearance results from vibrational temperatures, established just prior to the pulse peak, being very close to those at which maximum absorption occurs. Upon further heating, the increase in absorption is insufficient to cause a dip to occur at the pulse peak. The result is a transmitted pulse which is broadened to twice the input pulse duration. The model is also able to successfully predict the pulse shaping reported by Garside et al. [34] for a wide range of pressures and at temperature of 300 K. For both that case and for the results of the present experiments, the model is able to account for the pulse shaping observed even though strong intensity saturation processes result in transmission curves which are generally quite different from those involving only vibrational heating.

Perhaps the most significant result of the P(24) experiments is that the absorption behaviour at 450 K is very close to that predicted by the model in which only vibrational heating is considered.

This is shown in Fig. 5-4. The solid curve represents the predictions of the vibrational bath model. The small initial saturation quickly vanishes as more than 75% of absorption begins to occur from above 1500 cm^{-1}. This absence of saturation, at a pressure which shows strong saturation at 300 K, cannot be explained by the small changes in the collisional rates which accounted for the P(14) results. Rather, it supports the contention that the V-V relaxation rates are strongly dependent upon the location of the absorping levels in the vibrational bath.

5.5 Saturation Modelling

The results of the previous section suggest that the vibrational bath model can be used to predict SF_6 single pulse transmission even in the intensity saturation regime. A means of incorporating the vibrational energy dependence of the relaxation rates into the vibrational bath model is described below. Consider any two vibrational levels involved in an absorption as being separate from the remainder of the bath. The contribution of these levels to the total absorption can be obtained by solving the 2-level rate equations under steady-state conditions [59]. The absorption by these levels is a function of the input intensity I, and can be expressed as

$$\alpha_i(I) = \frac{\alpha_{o_i}}{1 + {}^{I}/I_{s_i}} \quad , \tag{5-1}$$

where α_{o_i} is the contribution to the small signal absorption coefficient. The intensity saturation parameter is defined by

$$I_{s_i} = h\nu A_{VV_i}/\sigma_i \quad . \tag{5-2}$$

Fig. 5-4

Transmission of SF_6 as a function of input intensity at the P(24) CO_2 line, and at 450 K. The SF_6 pressure at 300 K is 5 Torr. The solid curve represents the bath model predictions in the absence of saturation.

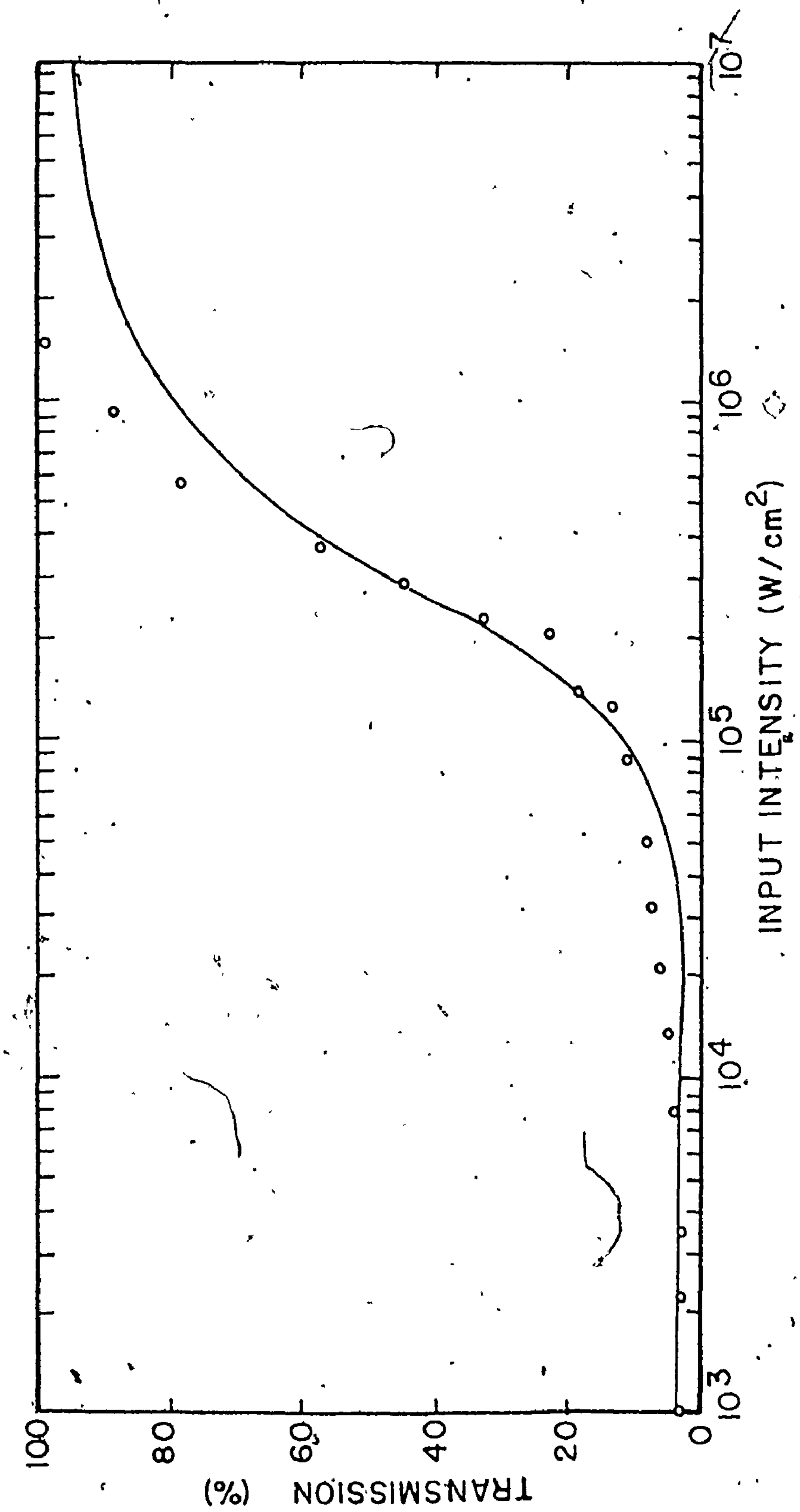
TRANSMISSION (%)
100
80
60
40
20
0
INPUT INTENSITY (W/cm^2)
10^3
10^4
10^5
10^6
10^7

where σ_i is the absorption cross-section (described in Section 2.2). The term A_{VV_i} represents the total vibrational equilibration rate between these levels. It is not necessarily equal to the more commonly quoted V-V relaxation rate, but rather represents the rate at which both the upper and lower levels couple into the bath. An explicit expression for A_{VV_i} is

$$A_{VV_i} = A_C(P) + A_{NC}(E_V) \quad . \tag{5-3}$$

The first term here is a collisional rate. For simplicity, it is chosen to depend only on the pressure, P, and not on the degree of vibrational excitation, hence

$$A_C(P) = C_1 P \quad . \tag{5-4}$$

P is the SF_6 pressure (in Torr) and C_1 a constant to be determined. The second term in Eq. (5-3) represents a collisionless exchange rate. It is assumed to be dependent only on the density of states, $N(E_V)$, which itself is a rapidly increasing function of vibrational energy E_V. Therefore,

$$A_{NC}(E_V) = C_2 \, [N(E_V)]^{\gamma} \quad , \tag{5-5}$$

where C_2 and γ are two other constants to be determined. No significance is given to the functional form here. It is chosen solely as a convenient way to describe the strong dependence of the collisionless relaxation rates on the density of states and hence, on the vibrational energy.

The total absorption can now be determined by summing the contributions, $\alpha_i(I)$, from each level in the vibrational bath. The parameter

C_1 is obtained by fitting the model predictions to the transmission measurements on the P(14) line, as described by Garside et al. [34]. The saturation behaviour shows no dependence on the non-collissional term since the P(14) absorption occurs from levels below 1500 cm^{-1}, a region in which the density of states is relatively small. After obtaining C_1 in this manner, measurements were performed at the P(26) CO_2 line at 300 K and values of C_1 and γ were obtained by fitting the bath model predictions to these results. The final values were $C_1 = 1.0 \times 10^5$ sec^{-1} $Torr^{-1}$, $C_2 = 5 \times 10^6$ (for E_V in cm^{-1} and σ_i in cm^2), and $\gamma = 4.$* Figure 5-5 shows the model predictions for the data of Garside et al. [34] on the P(14) CO_2 laser line. The solid curves represent the bath model predictions. Figure 5-6 illustrates similar results for the P(26) line. It can be seen that the essential features of the saturation behaviour can be accounted for; most notable are the reasonable predictions of the unusual shapes of the P(26) transmission curves. Although the agreement between theory and experiment is not as good as for the high pressure case described in Chapter 3, no model previously reported is applicable over such a wide range of SF_6 pressures and CO_2 wavelengths. The results further support the strong dependence of the vibrational relaxation rates on the vibrational energy. Future experimental work on the saturation behaviour, particularly that related to very short pulses, is necessary to determine a more accurate expression

---

*The bath model predictions for the P(14) case are found to be quite sensitive to the value of C_1; a change of 20% gives substantially different results. The calculations are much less sensitive to the value values of C_2 and γ.

Fig. 5-5

Transmission of SF_6 as a function of input intensity at the P(14) CO_2 line, and at 300 K. The data (from Garside et al. [34]) corresponds to SF_6 gas pressures of 10 Torr (x), 25 Torr (▲), 50 Torr (o) and 100 Torr (●). The solid curves represent the bath model predictions with the inclusion of saturation effects.

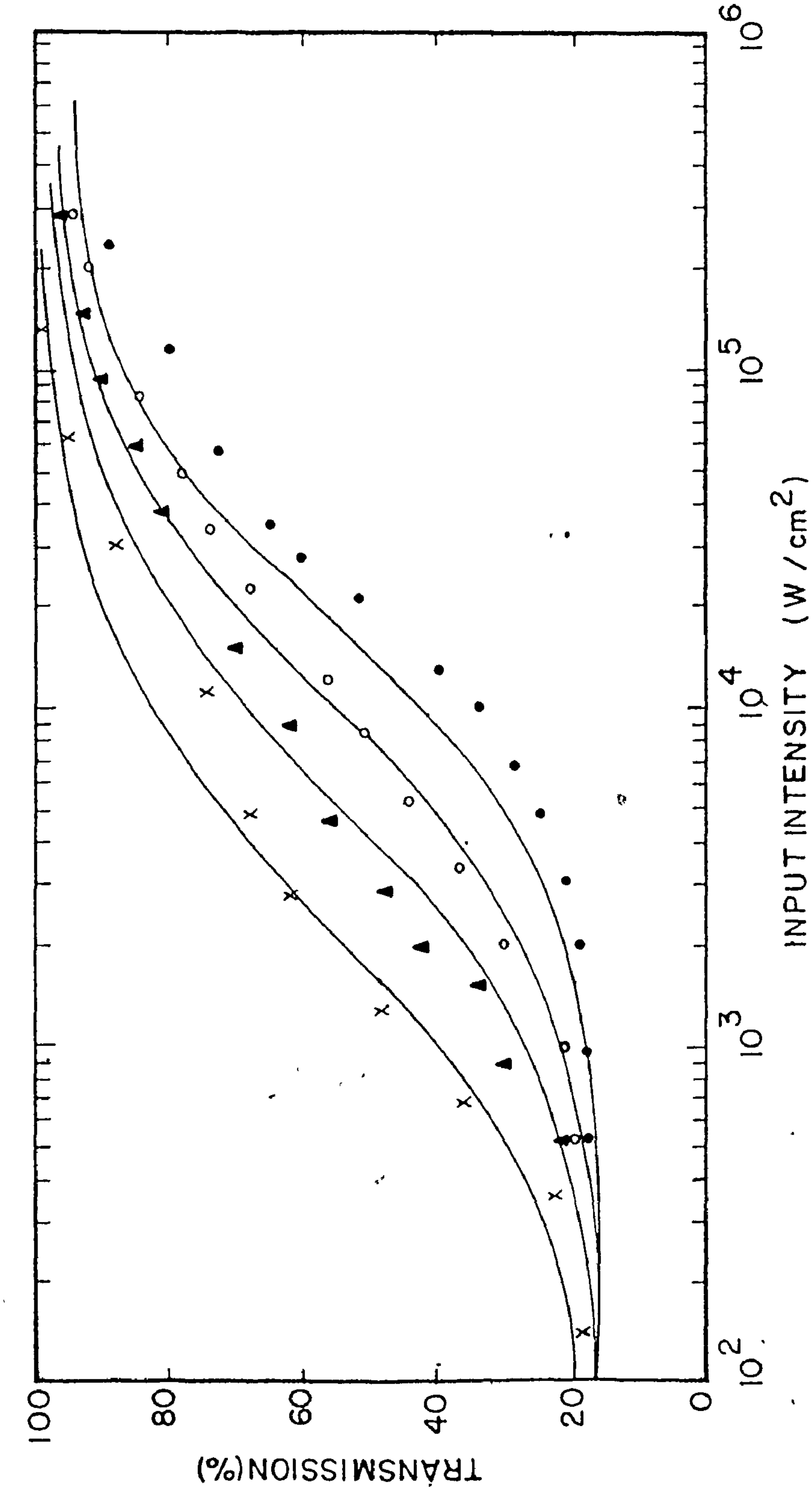

TRANSMISSION (%)
100
80
60
40
20
0
10^2
10^3
10^4
10^5
10^6
INPUT INTENSITY (W / cm^2)

Fig. 5-6

Transmission of SF_6 as a function of input intensity, at the P(26) CO_2 line, and at 300 K. The data corresponds to SF_6 gas pressures of 10 Torr (•), 30 Torr (▲), and 50 Torr (x). The solid curves represent the bath model predictions with the inclusion of saturation effects.

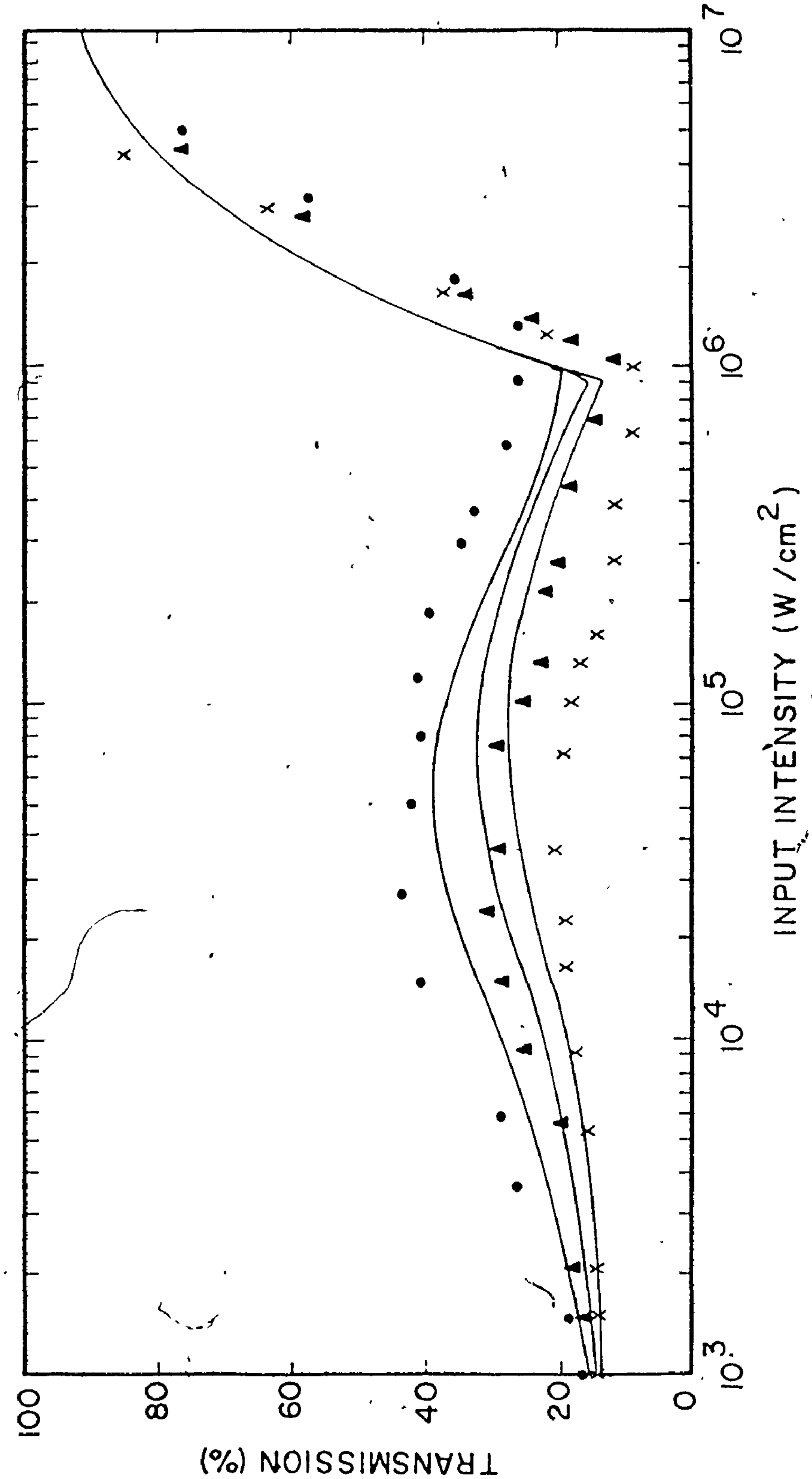
TRANSMISSION (%)
100
80
60
40
20
0
INPUT INTENSITY (W/cm²)
10³
10⁴
10⁵
10⁶
10⁷

for the non-collisional rate. Such refinements would certainly improve the success of the model when applied to situations involving strong intensity saturation.

5.6 Summary

This chapter has dealt with the extension of the vibrational bath model to the regions in which saturation effects become significant. Experiments with SF_6 at different initial temperatures determine the overall dependence of vibrational relaxation rates on the vibrational energy. The strong dependence of these rates on the degree of excitation is consistent with recently observed collisionless relaxation processes in SF_6 [57]. By relating this dependence to the density of states, a simple model can be constructed which predicts the essential features of single pulse transmission over a wide range of CO_2 wavelengths and SF_6 pressures. Further work is necessary to determine the exact dependence of these rates on the vibrational energy.

CHAPTER 6

CONCLUSIONS

The vibrational bath model developed in this thesis is able to predict the absorption behaviour of SF_6 at the 10.6 μm band of CO_2. This chapter summarizes the general features of the model and outlines the important conclusions resulting from the research. The applicability of the model to mode-locking and optical isolator design is discussed.

The introduction describes the importance of SF_6 as a saturable absorber for CO_2 laser systems. Yet despite the extensive use of SF_6, the actual absorption processes of the molecule are not completely understood. In particular, previous investigations have been unable to explain fully the strong dependence of the absorption on SF_6 pressure and CO_2 laser wavelength. The present model takes into consideration the multitude of vibrational and rotational levels that participate in the SF_6 absorption process. Furthermore, it does not require the use of numerous adjustable parameters characteristic of much of the previous work. The remarkable success achieved in the initial applications of the vibrational bath model provides strong support for its overall validity.

Chapter 2 describes the development of the basic model. The major assumption made is that a vibrational equilibrium can be maintained for a typical CO_2 laser pulse. It is shown that the basic model provides the proper dependence of the absorption on the vibrational temperature and can also account for the dynamics of the absorption. Previously reported V-V relaxation rates (as summarized in Chapter 5) would suggest that vibrational equilibrium cannot be maintained at low SF_6 pressures. Hence, the successful application of the model to these pressures is particularly significant.

Chapter 3 demonstrates the ability of the model to predict the transmission behaviour of CO_2 laser pulses through high pressure SF_6. The reduction in the absorption at high input intensities, which has the appearance of being intensity saturation, is in fact due to vibrational heating. Since this heating is a result of energy being absorbed from the laser pulse, these effects are energy rather than intensity dependent. Thus, the exact behaviour will depend on the laser pulse durations. However, the range of pulse durations for which the vibrational bath model is expected to apply is very large due to the rapid relaxation processes observed in SF_6.

The effects of dissociation on SF_6 absorption are discussed in Chapter 4. The amount of vibrational heating which occurs is limited by the maximum energy that an SF_6 molecule can possess before undergoing rapid dissociation. By incoporating this into the bath model it can successfully predict the observed dissociation and the corresponding effect on the transmission of CO_2 laser pulses through SF_6.

Chapter 5 discusses the extension of the vibrational bath model to the intensity saturation regime. Experimental evidence supports the strong dependence of the vibrational relaxation rates on the position in the bath of the particular states involved in the absorption. The rapid rates account for the persistence of heating effects even in situations where strong intensity saturation is plainly evident. An approximate but effective means is described for incorporating these effects into the vibrational bath model. It is then shown that the model can predict the basic features of the observed saturation behaviour.

It is clearly evident that two different mechanisms are responsible for the absorption behaviour of SF_6. The first is intensity saturation, which occurs at low SF_6 pressures, and is more apparent for the lower J-value CO_2 laser lines. The second mechanism is vibrational heating which is more prevalent at high SF_6 pressures and high J-value CO_2 lines. It has been shown that both processes can lead to a sharp reduction in absorption. However, the time required for the absorption to *recover* is the crucial difference between the two. For intensity saturation, the recovery time, which is of the order of the V-V relaxation times discussed in Section 5.1, is relatively fast. Absorption that has been reduced by vibrational heating can only recover when the vibrational temperature decreases. This occurs through V-T relaxation which requires a considerably longer time than the V-V processes. Hence,it is imperative that absorbers used in applications which require rapid recovery of the absorption operate in the intensity saturation regime.

The uses of SF_6 as an optical isolator and in particular as a passive mode-locker are excellent examples of such applications. The vibrational bath model greatly improves the understanding of mode-locking of CO_2 lasers with SF_6, as demonstrated in Ref. [37]. The bath model can also assist in selecting the components of gas isolator mixtures. For example, the model indicates that the onset of vibrational heating, and hence the lack of any true intensity saturation, may seriously hinder the effectiveness of SF_6 in high pressure gas isolator mixtures.

In conclusion, this thesis describes the development and experimental validation of a model which can determine the absorption behaviour of SF_6 in a variety of applications, and over a wide range of operating conditions. In addition, the model is applicable to many of the other large polyatomic molecules which interact with high powered CO_2 laser radiation. Consequently it is hoped that the research described in this thesis will be of considerable value to the design of CO_2 laser systems which employ large polyatomic molecules as saturable absorbers.

APPENDIX

Application of the Whitten-Rabinovitch Approximation

The Whitten-Rabinovitch approximation [25] is a method used to determine the density of states of large polyatomic molecules. The expression for $W(E_V)$, the total number of vibrational states below an energy E_V, is

$$W(E_V) = \frac{(E_V + aE_Z)^s}{s!\ \Pi_i\ h\nu_i} \quad , \tag{A-1}$$

and the corresponding expression for the density of states, $N(E_V)$, at a vibrational energy E_V is

$$N(E_V) = \frac{(E_V + aE_Z)^{s-1}}{(s-1)!\ \Pi_i\ h\nu_i} \quad . \tag{A-2}$$

Parameter s is the total number of degrees of freedom (15 for SF_6) and the ν_i are the fundamental vibrational frequencies. E_Z, the total zero point vibrational energy of all s modes, is given by

$$E_Z = \frac{1}{2} \sum_{i=1}^{s} h\nu_i \quad , \tag{A-3}$$

and is equal to 4677 cm^{-1} for SF_6. Factor a is an empirical parameter given by

$$a = 1 - \beta W(E') \quad , \tag{A-4}$$

where

$$\beta = \frac{s - 1}{s} \frac{\langle\nu^2\rangle}{\langle\nu\rangle^2} \quad . \tag{A-5}$$

In this expression, $\langle\nu^2\rangle$ and $\langle\nu\rangle$ are the mean square and mean frequencies of the molecule. The empirical function W(E') is expressed by

$$W = (5.00\, E' + 2.73\, E'^{\,0.50} + 3.51)^{-1} \quad (0.1 < E' < 1.0)$$

and (A-6)

$$W = \exp(-2.419\, E'^{\,0.25}) \quad , \quad (E' > 1.0)$$

where

$$E' = E_V / E_Z \tag{A-7}$$

is the reduced energy.

Whitten and Rabinovitch have demonstrated that negligible errors occur at energies above E' = 1 [60]. For SF_6, the errors become quite small above E' = 0.5 (∿2000 cm^{-1}). Therefore the Whitten-Rabinovitch approximation was employed for vibrational energies above 2000 cm^{-1}. The degeneracies (defined in Section 2.2) at these energies can be calculated using either Eq. (A-1) or Eq. (A-2). It was suggested by Nowak and Lyman [29] that the average values of the vibrational quantum numbers can also be obtained by the same approximation methods. For example, the average value of the quantum number v_3, in an energy level E_V, can be calculated by defining a factor

$$f\,(v_3,\,E_V) = \frac{N(E_V - v_3\nu_3,\, s = 12)}{N(E_V,\, s = 15)} \quad , \tag{A-8}$$

which is the fraction of molecules of vibrational energy E_V having v_3 quantum of ν_3. The denominator in Eq. (A-8) is simply the density of states at energy E_V. The numerator refers to the density of states at the energy $(E_V - v_3\nu_3)$ for which the ν_3 mode has been "frozen out" (i.e., s = 12). The average number of ν_3 quanta in the level E_V is

$$\bar{v}_3 = \frac{1}{\nu_3} \sum_{v_3} F(v_3,\, E_V)\, E_V \quad . \tag{A-9}$$

The summation is evaluated over all values of v_3 for which $v\nu_3 \leq E_V$.

The vibrational frequencies (ν_i, i = 1,6) are obtained from Ref. [24] and are (in cm^{-1}), 773.6 (1), 642.1 (2), 947.97 (3), 615.0 (3), 522.9 (3) and 346 (3). The numbers in brackets are the degeneracies of the modes. Values for the degeneracy $g(E_V)$ and the quantum numbers $\{v_i\}$ can now be assigned to all levels in the vibrational bath and then these in turn used to calculate the SF_6 absorption, as is described in Section 2.2.

REFERENCES

1. P.W. Smith, M.A. Duguay and E.P. Ippen, "Mode-locking of Lasers", in Progress of Quantum Electronics, edited by J.H. Sanders and S. Stenholm (Pergamon, Oxford, 1974), Vol. 3.
2. O.R. Wood and S.E. Schwarz, Appl. Phys. Lett., 12, 263 (1968).
3. A.J. Beaulieu, Appl. Phys. Lett., 16, 504 (1970).
4. R. Fortin, F. Rheault, J. Gilbert, M. Blanchard, and J.L. Lachambre, Can. J. Phys., 51, 414 (1973).
5. M.D. Montgomery, R.L. Carlson, D.E. Casperson, S.J. Czuchlewski, J.F. Figueira, R.F. Haglund, J.S. Ladish, A.V. Nowak and S. Singer, Appl. Phys. Lett., 32, 324 (1978).
6. S.J. Czuchlewski, A.V. Nowak, E. Foley, and J.F. Figueira, Opt. Lett., 2,39 (1978).
7. A.J. Alcock and A.C. Walker, Appl. Phys. Lett., 25 299 (1974).
8. A.F. Gibson, C.A. Rosito, C.A. Raffo, and M.F. Kimmitt, Appl. Phys. Lett., 21, 356 (1972).
9. V. Wang, C.R. Giuliano, S.D. Allen, R.C. Pastor, Proc. of a Symposium on Laser Induced Damage in Optical Materials, Boulder, Colo. U.S.A., 29-31 July 1975, (Washington, D.C., U.S.A.: Nat. Bur. Stand. 1976) page 118-125.
10. M.M. Delichatsios, H.W. Friedman and M. Sirchis, Technical Digest IEEE/OSA: Inertial Confinement Fusion, Topical Meeting, San Diego, Calif., U.S.A., Feb. 7-9, 1978.

11. P. Lavigne, J. Gilbert and J.L. Lachambre, Opt. Commun., 14, 194 (1975).

12. R.T.V. Kung and M. Sirchis, Appl. Phys. Lett., 32, 38 (1978).

13. R.T.V. Kung and M. Sirchis, Appl. Phys. Lett., 32, 206 (1978).

14. N.R. Isenor and M.C. Richardson, Appl. Phys. Lett., 18, 224 (1971).

15. J.L. Lyman, S.D. Rockwood, and S.M. Freund, J. Chem. Phys., 67, 4545 (1977).

16. J.L. Lyman, R.J. Jensen, J. Rink, C.P. Robinson, and S.D. Rockwood, Appl. Phys. Lett., 27, 87 (1975).

17. J.J. Armstrong and O.L. Gaddy, IEEE J. Quantum Electron., 8, 797 (1972).

18. Y.J. Kaufman, S. Ruschin, and U.P. Oppenheim, Appl. Opt., 16, 1187 (1977).

19. D.S. Frankel, Jr., J. Chem. Phys. 65, 1696 (1976).

20. R.S. Taylor, T.A. Znotins, E.A. Ballik, and B.K. Garside, J. Appl. Phys., 48, 4435 (1977).

21. K. Fox, Opt. Commun., 19, 397 (1976).

22. G. Herzberg, Infrared and Raman Spectra of Polyatomic Molecules, (Van Nostrand Reinhold Co., New York, N.Y., 1945).

23. W.H.J. Childs and H.A. Jahn, Proc. R. Soc. Lond., 169A, 451 (1939).

24. R.S. McDowell, J.P. Aldridge, and R.F. Holland, J. Phys. Chem., 80, 1203 (1976).

25. P.J. Robinson and K.A. Holbrook, Unimolecular Reactions, (Wiley-Interscience, 1972).

26. N. Bloembergen, C.D. Cantrell, and D.M. Larsen, "Collisionless Dissociation of Polyatomic Molecules by Multiphoton Infrared Absorption",

in Tunable Lasers and Applications edited by A. Mooradian, T. Jaeger and P. Stokseth (Springer-Verlag, Berlin, 1976) page 162.

27. H. Stafast, W.E. Schmid, and K.L. Kompa, Opt. Commun., 121 (1977).

28. C.C. Jensen, W.B. Person, B.J. Krohn, and J. Overend, Opt. Commun., 20, 275 (1977).

29. A.V. Nowak and J.L. Lyman, J. Quant. Spectrosc. Radiat. Transfer, 15 945 (1975).

30. R.V. Ambartzumian, Yu. A. Gorokhov, V.S. Letekhov, G.N. Makarov, and A.A. Puretskii, JETP Lett., 23, 22 (1976).

31. N.G. Basov, V.T. Galochkin, A.N. Oraevskii, and N.F. Starodubtsev, JETP Lett., 23, 521 (1976).

32. C.B. Moore, J. Chem. Phys., 43, 2979 (1965).

33. J.T. Knudtson and G.W. Flynn, J. Chem. Phys., 58, 1467 (1973). See also, R.D. Bates, Jr., J.T. Knudtson, G.W. Flynn, and A.M. Ronn, Chem. Phys. Lett., 8, 103 (1971).

34. B.K. Garside, R.S. Taylor, and E.A. Ballik, Can. J. Phys., 55, 849 (1977).

35. W. Frie, Zeitschrift für Physik, 201, 269 (1967).

36. A.V. Nowak, 1977. Private communication.

37. R.S. Taylor, Ph.D. thesis, McMaster University, 1978.

38. E.A. Ballik, B.K. Garside, R.S. Taylor and T.A. Znotins, Can. J. Phys., 55, 1956 (1977).

39. J.F. Bott and T.A. Jacobs, J. Chem. Phys., 50, 3850 (1969).

40. V.S. Letokhov and C.B. Moore, Sov. J. Quant. Electron., 6, 259 (1976).

41. J.P. Aldridge, J.H. Birely, C.D. Cantell, and D.C. Cartwright, "Experimental and Theoretical Studies of Laser Isotope Separation", in Physics of Quantum Electronics, Vol. 4 (1976) page 57.

42. E.R. Grant, M.J. Coggiola, Y.T. Lee, P.A. Schulz, Aa. S. Sudbo, and Y.R. Shen, Chem. Phys. Lett., 52, 595 (1977).

43. J.L. Lyman and S.D. Rockwoood, Opt. Commun., 18, 29 (1976).

44. D. Tal, U.P. Oppenheim, G. Koren, and M. Okon, Chem. Phys. Lett., 48, 67 (1977).

45. J. Dupré, P. Pinson, J. Dupré-Marquaire, C. Meyer, and P. Barchewitz, C.R. Acad. Sc. Paris, 282-B, 357 (1976).

46. C.R. Quick and C. Wittig, Chem. Phys. Lett., 48, 420 (1977).

47. J. Reid, B.K. Garside, and E.A. Ballik, IEEE J. Quantum Electron., 8, 449 (1972).

48. M.C. Gower and K.W. Billman, Opt. Commun., 20, 123 (1977).

49. G. Nickless, Inorganic Sulfur Chemistry, (Elsevier Pub. Co., New York, U.S.A., 1968).

50. N.R. Isenor and M.C. Richardson, Opt. Commun., 3, 360 (1971).

51. K.J. Olszyna, E. Grunwald, P.M. Keehn, and S.P. Anderson, Tetrahed. Lett., 19, 1609 (1977).

52. A. Azman and A. Ocvirk, Spectrochmica Acta, 23A, 1597 (1967).

53. G. Herzberg, Spectra of Diatomic Molecules, (Van Nostrand Reinhold Co., New York, N.Y., 1950).

54. Z. Karny and R.N. Zare, Chem. Phys., 23, 321 (1977).

55. J.G. Black, E. Yablonovitch, N. Bloembergen, and S. Mukamel., Phys. Rev. Lett., 38, 1131 (1977).

56. J.I. Steinfeld, I. Burak, D.G. Sutton, and A.V. Nowak, J. Chem.

Phys., 52, 5421 (1970).

57. T.F. Deutsch and S.R. Brueck, Chem. Phys. Lett., to be published.

58. C.D. Cantrell and H.W. Galbraith, Opt. Commun., 21, 374 (1977).

59. M. Hercher, Appl. Opt., 6, 947 (1967).

60. G.Z. Whitten and B.S. Rabinovitch, J. Chem. Phys., 38, 2466 (1963).